Thesis for the degree of Doctor of Philosophy

Aircraft Noise Prediction: from Trajectory to Synthesis

Evangelia Maria Thoma

Department of Mechanics and Maritime Sciences
CHALMERS UNIVERSITY OF TECHNOLOGY
Göteborg, Sweden 2024

Aircraft Noise Prediction: from Trajectory to Synthesis
Evangelia Maria Thoma
ISBN 978-91-8103-014-3

Doktorsavhandlingar vid Chalmers tekniska högskola
Ny serie nr 5472
ISSN 0346-718X

Department of Mechanics and Maritime Sciences
Chalmers University of Technology
SE–412 96 Göteborg, Sweden
Telephone + 46 (0) 31 – 772 1000

Printed by Chalmers Reproservice
Göteborg, Sweden 2024

Στον αδελφό μου.

Abstract

Aircraft Noise Prediction: from Trajectory to Synthesis
Thesis for the Degree of Doctor of Philosophy in Thermo and Fluid Dynamics
Evangelia Maria Thoma
Department of Mechanics and Maritime Sciences
Chalmers University of Technology

The issue of aircraft noise gained significant attention with the introduction of turbojets in commercial flights during the early 1960s. This led to the establishment of a series of standards and regulations that contributed to the development of quieter aircraft and the reduction in community noise impact. Since then, the regulations have continuously evolved, with ongoing efforts to mitigate aircraft noise focusing on advancements in aircraft and engine design and on more efficient flight procedures.

An important factor in making effective design choices in these efforts is the early noise impact assessment, ideally not only through conventional metrics but also through perception-based evaluation. One of the objectives of this work was to develop an aircraft noise prediction framework, capable of performing such assessments. At its core, this framework consists of trajectory modelling with aircraft and engine design and performance evaluation, source noise prediction, and propagation to a receiver. Incorporating the calculation of noise contours provided a more accurate representation of community noise impact across entire areas, facilitating the evaluation of noise from various scenarios. Nevertheless, the implemented conventional metrics could not fully capture the sound characteristics and perceived annoyance. To address this limitation, auralization was used to synthesize the predicted noise into audible sounds, providing a deeper understanding of the perceived noise. This comprehensive framework, starting with trajectory modelling and concluding with noise synthesis, facilitated a thorough assessment of different scenarios and their noise impact.

The selected scenarios primarily focused on flight path management, but the possibility of noise reduction at the source during the early design stages of conventional aircraft was also explored. Through a system-level analysis, new propulsion system designs were established indicating improvement in noise and NO_x emissions, for a minimum penalty in fuel consumption. Additional mitigation possibilities were explored through the operational aspect, aiming to establish quieter procedures, particularly during approach, through procedure design and optimization. The operational aspect was further investigated using experimental data to examine how variations in flight parameters influence noise across different approach configurations. In most of the aforementioned studies, interdependencies between noise, CO_2, and non-CO_2 emissions were assessed, highlighting the importance of considering trade-offs to avoid counteracting the benefits of noise mitigation with adverse effects on air quality. Overall, it was demonstrated that significant reduction can be achieved by designing feasible procedures within the current regulatory frameworks.

Keywords: aircraft noise, semi-empirical model, trajectory modelling, noise mitigation, interdependencies, model validation, noise mapping, auralization, noise synthesis.

Acknowledgments

I would like to express my sincere gratitude to all those who have supported me during my Ph.D. studies. This would have not been possible without all of you.

I would like to start by thanking my main supervisor Tomas Grönstedt for giving me the opportunity to be a part of this project, but also for his trust, guidance and support, that helped me grow as a researcher. I would also like to thank my supervisor Xin Zhao for his invaluable support and belief in me. Our interesting discussions and your constructive feedback always helped to keep me motivated and improve my research. More importantly, my deepest thank you to both of you for your understanding and support during a difficult time. I am also grateful for the support I have received from my supervisor Evelyn Otero Sola, from KTH. Our discussions and, your input and guidance have been invaluable to me.

I want to express my deepest gratitude to Anders Johansson, from KTH, not only for the excellent collaboration but also for all the input and help I have received from him. Thank you for your patience and time. Furthermore, I would like to thank Ulf Tengzelius, from Aurskall Akustik AB, for the many interesting discussions and for his help, and Henrik Ekstrand and Ulrika Ziverts, from Novair, for their input and advice. Your support during the initial stages of my studies has been greatly appreciated.

I would like to express my gratitude to Roberto-Merino Martinez, from TU Delft. Thank you for sharing your knowledge with me and for being an excellent supervisor and friend the few months I was there. I learned a lot from you and I greatly value your feedback and appreciate your patience. I also want to extend my thanks to everyone in the ANCE group for warmly welcoming me and making me feel like a valued part of their team. A special shoutout to Camilo, Anandini, Federica, and Andrei for making it feel a little more like home.

I would further like to thank all my past and present colleagues in the department for creating such an inspiring working environment and, especially, my office mates (old and new) for all the nice moments both during and outside of work. An extra special thank you to Oliver, Debarshee and Martina for all your support these past months and for your beautiful friendship. I can't wait to see what comes next!

I would also like to extend my appreciation to all my wonderful friends who are scattered around the world. A special thank you to Nikoletta for all these amazing years of friendship, for our adventures and for always being there for me. Ioli, I cannot thank you enough for your support from day one of my arrival in Sweden and for all our beautiful experiences. Karen, thank you for being an amazing friend and for everything you have taught me. Fabiola, I am grateful for an amazing year in Sweden and for everything that has followed since. Leonida and Kiriko, thank you for bringing me a little bit of home in Sweden and in the Netherlands.

Last, but in no way least, I would like to thank my family. My father for always supporting my choices and for believing in me and my mother for being the kindest, most caring person and for always being by my side. I am also thankful to my brother, for being the strongest person I have ever known and the best brother I could have. Your support means everything to me!

This research work was financially supported by the Swedish Transport Admin-

istration, Trafikverket, through the CIDER project (TRV2019/95826) which is a cooperation between Chalmers University of Technology, Aurskall Akustik AB, Novair and KTH Royal Institute of Technology, under the CSA (Centre for Sustainable Aviation) at KTH Royal Institute of Technology, Stockholm. The author would also like to thank the ANT project, also part of the CSA, for providing the noise measurements, flight data and recordings that were used for the validation of the models.

Evangelia Maria Thoma
Göteborg, April 2024

List of Publications

This thesis is based on the following appended papers:

Paper 1. Evangelia Maria Thoma, Tomas Grönstedt, Xin Zhao. *Quantifying the Environmental Design Trades for a State-of-the-Art Turbofan Engine.* Aerospace 2020, 7, 148. https://doi.org/10.3390/aerospace7100148

Paper 2. Evangelia Maria Thoma, Tomas Grönstedt, Evelyn Otero, Xin Zhao. *Environmental Assessment of Noise Abatement Approach Trajectories.* 33rd ICAS Congress, September 4-9, 2022, Stockholm, Sweden.

Paper 3. Evangelia Maria Thoma, Tomas Grönstedt, Evelyn Otero, Xin Zhao. *Assessment of an Open-Source Aircraft Noise Prediction Model Using Approach Phase Measurements.* Journal of Aircraft 2023. https://doi.org/10.2514/1.C037332

Paper 4. Evangelia Maria Thoma, Anders Johansson, Xiaoyi Lin, Evelyn Otero. *Flight Configuration-Based Analysis of Emissions and Noise Interdependencies* Manuscript under review in Journal of Aircraft.

Paper 5. Evangelia Maria Thoma, Roberto Merino-Martínez, Tomas Grönstedt, Xin Zhao. *Noise from Flight Procedure Designed with Statistical Wind: Auralization and Psychoacoustic Evaluation.* Accepted and to be presented on the 30th AIAA/CEAS Aeroacoustics Conference and subsequently to be submitted to an AIAA journal for consideration.

Nomenclature

Roman symbols

a	Atmospheric absorption
	Argument of complex spherical-wave reflection coefficient (eq. 4.4)
a_{cl}	Classical absorption (eq. 4.3)
a_{ft}	Atmospheric absorption in dB per $1000ft$ (eq. 3.10)
a_i	i_{th} prediction parameter or equivalent jet state property (eq. 3.18)
a_{ir}	Standard value for the i_{th} prediction parameter (eq. 3.18)
a_{mol}	Molecular absorption (eq. 4.3)
a_{vib}	Absorption caused by vibrational relaxation processes (eq. 4.3)
a_0	Empirical coefficient (eq. 3.6)
a_1	Empirical coefficient (eq. 3.6)
a_2	Empirical coefficient (eq. 3.6)
a_3	Empirical coefficient (eq. 3.6)
A_i	Amplitude of the i_{th} tone (Chapter 5)
b	Empirical coefficient (eq. 3.7) / Wing or tail span
B	Number of blades in the turbine last rotor stage
c	Speed of sound
C	Coherence coefficient / Empirical parameter (eq. 3.4)
C_D	Drag coefficient
c_L	Speed of sound at the turbine exit
C_L	Lift coefficient
c/s	Stator-rotor spacing
D	Drag / Directivity index (eq. 3.16)
D_e	Equivalent diameter of the coaxial or circular jet
D_i	Respective length scale for landing gear components
E_{Eng}	Engine installation effects factor
f	Fuel flow (Chapter 2) / Frequency (Chapter 3)
f_b	Fan blade passage frequency
f_{max}	Frequency for maximum wing trailing-edge noise in airframe noise prediction method
f_r	Relaxation frequency
f_0	Fundamental blade passage frequency of the last stage of the turbine
F	1/3 octave band normalized power spectrum (eq. 3.16)
	Ground wave function (eq. 4.5)
F_C	Combustor flow function
F_s	Sampling frequency
F_1	Empirical function (eq. 3.1 and eq. 3.4) / Empirical function (eq. 3.12)
F_2	Empirical function (eq. 3.1 and eq. 3.4) / Empirical function (eq. 3.13)
F_3	Empirical function (eq. 3.1 and eq. 3.5)
F_4	Empirical function (eq. 3.2 and eq. 3.3)
g	Gravitational acceleration
G	Ground effects factor

h	Altitude / Filter signal in the time domain (Chapter 5)
h_m	Microphone height
H	Transfer function (Chapter 5)
H_{aa}	Atmospheric absorption filter transfer function (eq. 5.9)
K	Wave number (eq. 4.4)
k_0	Empirical coefficient (eq. 3.9)
k_1	Empirical coefficient (eq. 3.9) / Empirical coefficient (eq. 3.16)
k_2	Empirical coefficient (eq. 3.9) / Empirical coefficient (eq. 3.16)
k_3	Empirical coefficient (eq. 3.16)
K	Empirical correction factor (eq. 3.14) /
	Sub-band correction factor (eq. 4.4)
L	Lift (Chapter 2) / Block length (Chapter 5)
L_{Amax}	Maximum A-weighted sound pressure level
L_c	Peak characteristic sound pressure level for the fan
L_{den}	Day - evening - night yearly averaged sound pressure level
$L_{lateral}$	Sound pressure level in the lateral aircraft direction
L_{night}	Yearly averaged sound pressure level for the night
L_p	Sound pressure level
L_{pA}	A-weighted sound pressure level
L_{under}	Sound pressure level directly under the aircraft
L_0	Peak sound pressure level for the turbine
m	Aircraft mass
$\dot{m}$	Mass flow rate
M	Mach number / Filter length (Chapter 5)
M_{tr}	Rotor tip relative Mach number
M_{trd}	M_{tr} at fan design point
N	Number of samples or signal length (Chapter 5)
N_b	Number of sub-bands
N_f	Number of ignited fuel nozzles in the combustor
$N_{f,max}$	Total Number of DAC Fuel Nozzle
N_s	Number of landing gear main struts
N_t	Number of landing gear tires
p	Acoustic pressure
R	Turn radius (Chapter 2) /
	Distance between source and observer (Chapter 3) /
	Magnitude of complex spherical-wave reflection coefficient (eq. 4.4)
R_o	Observation radius for combustor noise prediction method
S	Wing or tail area in airframe noise prediction method /
	Suppression factor (eq. 3.26)
S_{dB}	Suppression in dB
St	Strouhal number
S_w	Aircraft reference area
t	Time
T	Thrust (Chapter 2) / Temperature (Chapter 3 and 4)
T_L	Turbine/Nozzle Acoustic Transmission Loss Parameter
V	True airspeed

V_e	Nozzle exit equivalent flow velocity
V_{GS}	Ground speed
V_l	Local airspeed
V_{TR}	Relative tip speed of the turbine last rotor
V_w	Wind speed
V_z	Vertical aircraft speed
W	Aircraft weight
x	Time domain signal (Chapter 5)
x_i	Equivalent jet flow properties
X	Signal in the frequency domain (Chapter 5)
y	Filtered signal (Chapter 5)
Y	Filtered signal in the frequency domain (Chapter 5)

Greek symbols

α	Angle of attack
γ	Flight path angle
Γ	Plane wave reflection coefficient
δ	Boundary layer thickness
Δ	Difference
Δ_i	Empirical constants (eq. 3.22)
ΔdB	Empirical correction function (eq. 3.15)
ΔSPL	Normalized SPL for each component (eq. 3.23)
η	Normalized frequency parameter for the jet
θ	Pitch angle (Chapter 2) / Longitudinal directivity angle (Chapter 3)
θ_p	Normalized longitudinal directivity angle
Λ	Total lateral attenuation
ν	Kinematic viscocity
ξ	Angle between direction of aircraft and sound propagation path
ρ	Density
ϕ	Roll or bank angle (Chapter 2) / Lateral directivity angle (Chapter 3)
ϕ_i	Initial phase for the i_{th} tone (Chapter 5)
ϕ_w	Wind direction
ψ	Heading angle
ω	Shaft rotational speed

Subscripts

0	Reference value
n	Normalized value
p	Peak value
s	Static value

Abbreviations

AEDT	Aviation Environmental Design Tool
ANOPP	Aircraft NOise Prediction Program
ANT	Approach Noise Trials
BLI	Boundary Layer Ingestion
BPF	Blade Passing Frequency
BPR	Bypass Ratio
CAA	Computational Aeroacoustics
CDA	Continuous Descent Approach
CFD	Computational Fluid Dynamics
CP	Cycle Parameter
CHOICE	CHalmers nOIse CodE
CIDER	CorrelatIon- and physics- based preDiction of noisE scenaRios
CSA	Center for Sustainable Aviation
DAC	Dual-Annular Combustor
DFT	Discrete Fourier Transform
END	Environmental Noise Directive
EPNL	Effective Perceived Noise Level
FAA	Federal Aviation Authority
FDR	Flight Data Recorder
FFT	Fast Fourier Transform
FIR	Finite Impulse Response
FPR	Fan Pressure Ratio
GESTPAN	GEneral Stationary and Transient Propulsion ANalysis
ICAO	International Civil Aviation Organization
IIR	Infinite Impulse Response
INM	Integrated Noise Model
LDLP	Low Drag Low Power
LTO	Landing and Take-Off
LG	Landing Gear
OASPL	Overall Sound Pressure Level
OASPLN	Overall Sound Pressure Level Normalized
OAPWL	Overall Sound Power Level
OPR	Overall Pressure Ratio
PANAM	Parametric Aircraft Noise Analysis Module
PNL	Perceived Noise Level
RNP AR	Required Navigation Performance Authorisation Required
RSL	Relative Spectrum Level
RSS	Rotor-Stator Spacing
SAC	Single-Annular Combustor
SAF	Sustainable Aviation Fuel
SEL	Sound Exposure Level
SFC	Specific Fuel Consumption
SPL	Sound Pressure Level

SPLN	Sound Pressure Level Normalized
SQAT	ound Quality Analysis Toolbox
TAS	True AirSpeed
WEICO	WEight and COst estimation
WHO	World Health Organization

Contents

Part I

Introductory Chapters

Chapter 1
Introduction

1.1 Background

Sound is a vibration that travels through a medium and can be heard when it reaches the ear of a person or an animal. It creates a means of communication between people and may even be a form of entertainment. In some cases, a sound can also be unpleasant or loud causing disturbances and annoyance. This form of unwanted or unpleasant sound is defined as noise and it can originate from a number of different sources, such as transportation, industry or leisure activities.

According to the World Health Organization (WHO), transportation noise is recognized as the second most important cause impacting public health in six European countries [1], [2]. This includes noise from road, rail and air traffic. Among these, aircraft noise, although affecting fewer people, is considered to be the most annoying [2]. Its impact is not limited to community annoyance, but includes several other effects on the human health and well-being, such as sleep disturbance, cognitive impairment in children and cardiovascular disease [1], [3], [4].

It is estimated that, in 2017, almost one million European citizens were highly annoyed by aircraft noise and more than two hundred thousand were highly sleep disturbed [5], [6], according to data reported by the Environmental Noise Directive (END) [7]. It is also estimated that about 0.8 % of the European population was exposed, during the entire day, to noise level above L_{den} 55 dB and, during the night time, one third of that was exposed to noise level above L_{night} 50 dB, while the recommended levels by WHO are 45 dB and 40 dB, respectively [2] (where L_{den} is the yearly averaged sound pressure level determined over the day, evening and night, with a penalty of 5 dB for the evening and 10 dB for the night, and L_{night} is the averaged sound pressure level for the night). These numbers continued to increase steadily until 2020, when the air traffic was significantly reduced due to the COVID 19 outbreak, and the exposed population dropped to about one third of the previous year. The aviation industry is, however, on a recovering path and an average annual growth of 0.9 %, as a baseline scenario, is expected in flights at European airports, for the period from 2019 to 2050 [5]. Despite this, fleet renewal is expected to reduce the average noise exposure in the following decades, even if the increase in air traffic is faster [5]. Nevertheless, aircraft noise is still a major concern

and if no further actions are taken the noise exposure indicators may soon increase again.

1.2 Aircraft noise regulations and mitigation

It is apparent that aircraft noise is still, and will continue to be, an important aspect of the environmental impact of the aviation industry and it should be dealt with on many levels. To that end, the International Civil Aviation Organisation (ICAO) has proposed a balanced approach to the problem of aircraft noise mitigation, that consists of four principle elements, including: reduction of noise at the source, land-use planning and management, noise abatement operational procedures, and operating restrictions [8].

Perhaps the most effective element of the balanced approach is the reduction of noise at the source. This has been realized by the setting of aircraft noise limits through noise certification procedures and standards, which ensure that the latest and most advanced noise reduction technologies are incorporated into the aircraft. These standards are defined in "Annex 16 - Environmental Protection - Volume I - Aircraft Noise" [9] and in "Doc 9501 - Environmental Technical Manual - Volume I - Procedures for the Noise Certification of Aircraft" [10] and include three reference certification points, namely, flyover or take-off, lateral or sideline, and approach. The flyover point is defined directly under the aircraft flight path and at 6.5 km from the start-of-roll; the lateral point is placed 450 m at the side of the runway, at the point where the noise level is maximum during take-off; the approach point is located 2 km from the runway threshold on the runway axis. From these points, noise measured at approach is usually the highest [11], [12] which is mainly driven by the reduced aircraft-microphone distance at this point, and the technological advancements in engine technology that have led to increasing airframe noise contribution. Although significant improvement can be achieved through novel aircraft concepts [13], [14], such as the silent aircraft initiative presented in Figure 1.1, and advanced or optimized engine designs [15]–[17], these are more long term solutions that would require replacing existing fleets and potentially airport infrastructure.

Figure 1.1: "Silent" aircraft concept. Reprinted from [18].

Efficient land-use planning and management is an important aspect of aircraft noise mitigation that complements the benefits of noise reduction at the source by introducing land-use zoning around airports. This includes airport development and

expansion at appropriate areas and aviation compatible land-use around airports, e.g. development of industrial areas instead of houses. These guidelines are described in ICAO Doc 9184 [19].

The third element recommended by ICAO's balanced approach is noise abatement operational procedures, which can be very effective, especially if adapted to specific aircraft, airports and conditions. Guidelines in this aspect include noise preferential runways and routes and the use of noise abatement procedures for approach and departure. The latter, namely, noise optimal procedures, is probably the most efficient way to reduce noise from existing aircraft, and it has been the topic of many research studies [20]–[25] which show that significant improvement can be achieved. However, near airport operations, i.e. departure and approach, are usually subject to several restrictions due to obstacles, safety considerations, crew workload, etc., and in many airports, there are pre-defined procedures that the aircraft must follow. These procedures are mainly designed based on the ICAO's recommendations through a number of flight operations manuals [26]–[31]. Nevertheless, such research efforts are necessary and should continue as flexibility in flight procedure design is improved with the advancement of communication and navigation equipment [32].

The final element, operating restrictions, is used to complement the benefits of the other three. It includes limiting and even banning the operation of the noisiest aircraft at certain airports, restrictions in night time operations, increased charges to noisy aircraft and other restrictions with regards to the nature of the flight

From the proposed elements, research on aircraft noise mitigation is mainly focused on the reduction of noise at the source, through investigation of novel concepts, design optimization of existing aircraft and engine, and development of noise reduction mechanisms, and improvements in flight procedures, mainly through flight path optimisation. To achieve the maximum benefit, a combination of measures would be ideal. However, independent of the scenario, interrelationships between different aspects, e.g. between noise and emissions, noise and passenger comfort, etc. should always be considered in order to achieve optimal and realistic results.

1.3 Noise and emissions mitigation goals and interdependencies

Of all the underlying interdependencies, noise and emissions is perhaps the most crucial. Aviation emissions, and especially CO_2 emissions, have been on the spotlight of the aviation industry's environmental impact, in the recent years, as they account for 4 % of the total CO_2 emissions in Europe and $2-3$ % globally [33]. That has led to the commitment of the aviation industry in Europe to reach net-zero greenhouse gas emissions by 2050 [33], meeting the European Union's goal for climate neutrality under the Paris Agreement [34], [35], while the aim in terms of noise is to achieve a 65 % reduction in perceived noise per operation, relative to 2000 [36]. In the shorter term, a 55% reduction in CO_2 emissions is aimed by 2030 and a 30% reduction in non-CO_2 emissions by 2035, compared to 1990 [5], [33], [36]. The number of people chronically disturbed by noise is expected to reduce by 30% by 2030, compared

to 2017, and the number of premature deaths due to air pollution by 55%, compared to 2005 [5]. Finally, it is intended that there will be no population growth in the L_{den} 65 dB and L_{night} 50 dB contours by 2035, compared to 2019, while insulation measures will be implemented for the population residing in these areas [36].

It becomes clear that these commitments require immediate action, through technological improvements, use of sustainable aviation fuels (SAF) and hydrogen, improved operations and flight procedures, and economic measures. In any of these measures, a detailed assessment of incurring trade-offs between noise, CO_2 and non-CO_2 emissions should be performed, in order to avoid adverse effects in other metrics.

1.4 Thesis objectives and outline

From the previous sections, it becomes apparent that there is still potential and need to further reduce aircraft noise. To that aim, the presented work is centered around exploring and assessing noise mitigation scenarios and opportunities. Fundamental for these studies is the development of an accurate prediction tool with the capability to assess the noise impact through different metrics, such as noise contours and auralization. In these scenarios, interdependencies with CO_2 and non-CO_2 emissions are often addressed to ensure that any proposed measure is in line with the goals set by the aviation industry. The selected scenarios follow the elements proposed by ICAO in the balanced approach, with a focus on the reduction of noise at the source and noise abatement operational procedures. Therefore, another objective was to develop a model that can be used to design and optimize flight trajectories, and assess the aircraft performance. This was coupled with an existing in-house engine performance model. A tool-chain was, thus, created, starting from the trajectory definition and aircraft and engine modelling, followed by the source noise prediction and propagation to a specified location or over an entire area, and finally, enhanced with auralization to be able to perform subjective assessment of proposed mitigation measures for the selected scenarios. Finally, an additional outcome of the work was the release of the aircraft source noise prediction code as an open-source tool, enabling its use and development by other researchers in the scientific community.

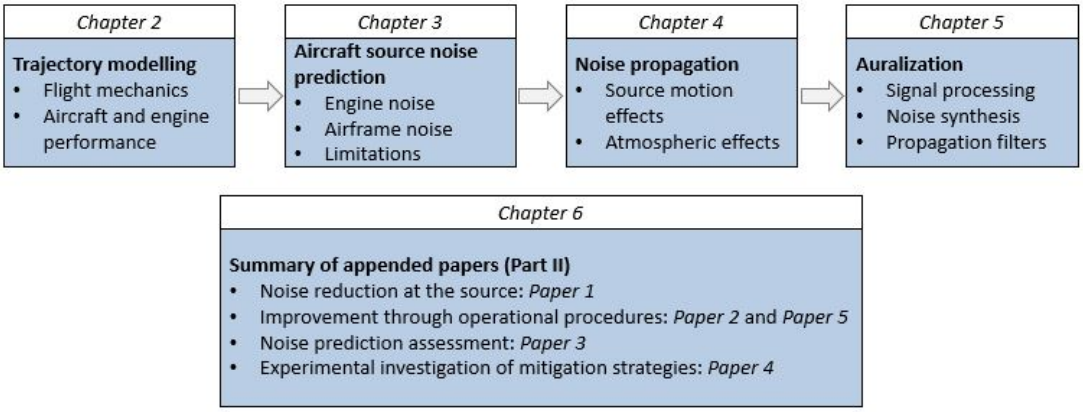

Figure 1.2: Outline of Introductory Chapters.

The thesis consists of two basic parts. The first part, referred as Introductory Chapters, forms an extended summary of the work related to the development of the noise prediction tool-chain, which composes the basis of the selected scenarios and performed studies. The second part, Appended Papers, contains the studies that were selected and performed in chronological order. The chapters included in the first part are outlined in Figure 1.2 and organized as follows: In Chapter 2 a detailed description of the trajectory performance model is presented, including flight mechanics and aircraft and engine performance modelling. Chapter 3 and Chapter 4 are dedicated to the description of the implemented source noise prediction models and the propagation methods that are used for estimating the noise on a selected microphone location or generating noise contours. The auralization procedure is described in Chapter 5. Finally, Chapter 6 provides a summary of the appended papers and Chapter 7 summarizes the key findings of the work and discusses possible aspects to be included in future research.

From the appended papers, Paper 1 focuses on the noise reduction at the source. More specifically, a system-level study was performed on a state-of-the-art turbofan engine to quantify the effect of early design choices on noise and NO_x emissions, for a minimum penalty in fuel burn. Paper 2 focuses on the evaluation of interdependencies between noise and emissions for standard, more advanced and optimized noise abatement approach procedures. In Paper 3, a comparative assessment of the source noise level prediction with backpropagated noise measurements from flyover aircraft was performed. The study was performed for all approach configurations, and included a sensitivity analysis relative to variations in flight parameters and an assessment of the predicted noise level on the ground. Paper 4 takes advantage of the same series of flyover noise measurement tests to investigate trade-offs between noise and emissions for the different stages of approach procedures and to identify mitigation techniques. Lastly, in Paper 5, two Required Navigation Performance Authorisation Required (RNP AR) approach procedures that were designed following the two design methodologies proposed in the ICAO regulations were assessed for their noise impact. The assessment was performed by comparing the two procedures in terms of sound exposure level contours, amount of affected population, auralization, and psychoacoustic metrics.

Chapter 2

Trajectory, Aircraft and Engine Modelling

Aircraft trajectory modelling is the starting point of any design or simulation process in aviation-related research. It is also an effective and one of the most direct ways through which the noise level on the ground can, to a certain extent, be controlled.

Designing noise optimal procedures requires accurate modelling of the aircraft and engine performance. This section is dedicated to the methods and tools that have been developed and used to generate and evaluate procedures and predict the aerodynamic and operational performance of the aircraft. The development was based on approach data and procedures but the methods described are applicable for all flight phases.

2.1 Flight dynamics

2.1.1 Equations of motion

The derivation of the dynamic equations describing the motion of the aircraft in three dimensions can be found in many flight mechanics books such as [37]. The general assumption is that all forces are acting on the center of mass of the aircraft and the velocity vector is considered in the plane of symmetry of the airplane, i.e. the sideslip angle is zero. The equations of motion for a flight over a flat earth are then given by

$$\begin{cases} T\cos(\alpha) - D - W\sin(\gamma) = m\dot{V} \\ (T\sin(\alpha) + L)\sin(\phi) = mV\cos(\gamma)\dot{\psi} \\ (T\sin(\alpha) + L)\cos(\phi) - W\cos(\gamma) = mV\dot{\gamma} \\ \dot{x} = V\cos(\gamma)\cos(\psi) \\ \dot{y} = V\cos(\gamma)\sin(\psi) \\ \dot{h} = V\sin(\gamma) \\ \dot{W} = -f \end{cases} \tag{2.1}$$

where T is the thrust for the total number of engines, α the angle of attack, D the drag, L the lift, ψ the heading or yaw angle, h the altitude, and f the fuel consumption. The airspeed, V and flight path angle, γ, are defined from the following equations

$$V = c_0 M \sqrt{\frac{T_s}{T_0}} \tag{2.2}$$

$$\gamma = \arcsin\left(\frac{V_z}{V}\right) \tag{2.3}$$

with $c_0 = 340.29\ m/s$ the reference speed of sound and $T_0 = 288.15\ K$ the reference temperature. M is the mach number, T_s the static temperature and V_z the vertical speed.

The first three equations in eq. 2.1 are derived based on the $(x_1 - y_1 - z_1)$ axis system and the rest based on the ground axis system $(x - y - z)$ presented in Figure 2.1. The attitude angles γ, ϕ and ψ are also shown in the same figure.

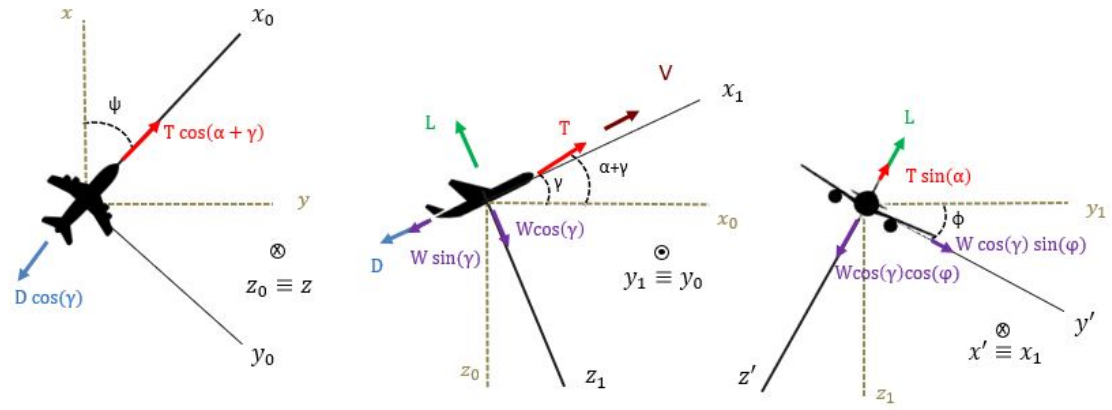

Figure 2.1: Coordinate system and aircraft free body diagram in three dimensions.

2.1.2 Equations of motion with wind

The movement of the aircraft and its trajectory while on the air are controlled using the control devices on the aircraft, e.g. ruder, slats, flaps etc. However, one key factor that can alter the aircraft's path is the wind. Wind speed and direction can have a significant effect on the flight, and it is important to consider them when planning routes.

When the aircraft is flying in crosswind conditions, it tends to deviate from its actual or desired path. This deviation is called drift and is defined as the angle between the aircraft heading, the direction in which the nose of the aircraft is pointing, and its track, the direction in which the aircraft is actually going. In order to maintain the aircraft in the desired course, its heading must be corrected depending on the wind speed and direction. The angle that the aircraft must be turned is referred as wind correction angle. It is often assumed that the drift and the wind correction angle are equal. While in some cases this might be true, they are not the same angle by definition as explained by Alexander and Klose [38]. Finally, in the case that the

wind and aircraft velocity vectors are parallel, the heading and the track coincide, and if they are pointing in the same direction, the phenomenon is called tailwind, while if they have opposite directions, it is called headwind.

With the inclusion of wind, there are two velocity vectors that are used to describe the motion of the aircraft. The first is TAS (True Airspeed), which is the velocity of the aircraft relative to the air. In this thesis, true airspeed is symbolised with V and it can be derived directly from the Mach number according to eq. 2.2. The second velocity vector is GS (Ground Speed), which is defined as the velocity of the aircraft relative to the ground. Ground speed can be determined from true airspeed with a simple vector addition with the wind velocity, as indicated by eq. 2.4.

$$\overrightarrow{V}_{GS} = \overrightarrow{V} + \overrightarrow{V}_{w} \tag{2.4}$$

where the wind velocity is written relative to the ground axis system as

$$\overrightarrow{V}_{w} = V_{wx}\vec{i} + V_{wy}\vec{j} + V_{wz}\vec{k} \tag{2.5}$$

Wind direction data are usually provided relative to true north, i.e. wind direction equal to 0^o corresponds to wind blowing from north to south. For the calculations and for the equations that will be presented it is adjusted and refers to the angle between the wind velocity vector and the true airspeed.

For the derivation of the three-dimensional dynamic equations of motion for the case of flight in wind, only horizontal wind was considered, but a vertical component can easily be incorporated. The equations of motion in this case are derived using the absolute acceleration of the aircraft relative to the ground.

$$\overrightarrow{F} = m\overrightarrow{\dot{V}_{GS}} = m\left(\overrightarrow{\dot{V}} + \overrightarrow{\dot{V}_{w}}\right) \tag{2.6}$$

The acceleration of the aircraft relative to the air from eq. 2.1 and Figure 2.1 is defined as

$$\overrightarrow{\dot{V}} = \dot{V}\vec{i_1} + V\cos(\gamma)\dot{\psi}\vec{j_1} - V\dot{\gamma}\vec{k_1} \tag{2.7}$$

The acceleration of the wind, accounting only for the horizontal components, is derived from eq. 2.5 as

$$\overrightarrow{\dot{V}_{w}} = \dot{V}_{wx}\vec{i} + \dot{V}_{wy}\vec{j} + V_{wx}\frac{d\vec{i}}{dt} + V_{wy}\frac{d\vec{j}}{dt} \tag{2.8}$$

with $V_{wx} = V_w\cos(\psi + \phi_w)$ and $V_{wy} = V_w\sin(\psi + \phi_w)$

However, the ground axis system is always fixed relative to the earth and therefore invariable with time. Thus, eq. 2.8 becomes

$$\overrightarrow{\dot{V}_{w}} = \dot{V}_{wx}\vec{i} + \dot{V}_{wy}\vec{j} \tag{2.9}$$

Using rotational matrices eq. 2.9 can be rewritten relative to the body axis system.

$$\begin{aligned}\overrightarrow{\dot{V}_{w}} = \left(\dot{V}_{wx}\cos(\psi) + \dot{V}_{wy}\sin(\psi)\right)\cos(\gamma)\vec{i_1} + \left(-\dot{V}_{wx}\sin(\psi) + \dot{V}_{wy}\cos(\psi)\right)\vec{j_1} \\ + \left(\dot{V}_{wx}\cos(\psi) + \dot{V}_{wy}\sin(\psi)\right)\sin(\gamma)\vec{k_1}\end{aligned} \tag{2.10}$$

Then, eq. 2.1 becomes

$$\begin{cases} \dot{V} = \frac{1}{m}\left(T\cos\left(\alpha\right) - D - W\sin\left(\gamma\right)\right) - \dot{V}_{wx_1} \\ \dot{\psi} = \frac{1}{mV\cos\left(\gamma\right)}\left(T\sin\left(\alpha\right) + L\right)\sin\left(\phi\right) - \frac{\dot{V}_{wy_1}}{V\cos\left(\gamma\right)} \\ \dot{\gamma} = \frac{1}{mV}\left(\left(T\sin\left(\alpha\right) + L\right)\cos\left(\phi\right) - W\cos\left(\gamma\right)\right) - \frac{\dot{V}_{wz_1}}{V} \\ \dot{x} = V\cos\left(\gamma\right)\cos\left(\psi\right) + V_w\cos\left(\psi + \phi_w\right) \\ \dot{y} = V\cos\left(\gamma\right)\sin\left(\psi\right) + V_w\sin\left(\psi + \phi_w\right) \\ \dot{h} = V\sin\left(\gamma\right) \\ \dot{W} = -f \end{cases} \tag{2.11}$$

where $\dot{V}_{wx'}$, $\dot{V}_{wy'}$ and $\dot{V}_{wz'}$ are the components in eq. 2.10.

2.2 Trajectory modelling

In this work, trajectories are constructed as a series of points and segments. The model starts from the definition of the horizontal flight path which can either follow a pre-defined ground path or be constructed by defining control points. These points are then connected with straight or curved segments with a specified turn radius. In the latter case, the bank angle of the aircraft can be calculated as

$$\phi = \arctan\left(\frac{V^2}{gR}\right) \tag{2.12}$$

where V is the aircraft speed, g is the gravitational acceleration and R is the turn radius.

The vertical profile can, then, be built by assigning a combination of flight parameters to each selected point. These parameters can include, for example, altitude, speed and flight path angle or horizontal distance, speed, flight path angle and acceleration. A sample parameterization defined in this way for an approach trajectory is presented in Figure 2.2, where V is the speed, h the altitude, s the horizontal distance and γ the flight path angle. The required configuration changes (flap and slat deflection and landing gear extensions), if relevant, can also be provided in terms of distance, altitude, speed, or time.

Depending on the selected parameterization, the speed between two consecutive points is calculated from the provided acceleration or assuming a linear variation with distance or time. Assuming a constant flight path angle between waypoints, the rest of the trajectory parameters, namely altitude, distance or flight path angle, can easily be computed, following the basic relationships introduced in Section 2.1. Thus, all the required parameters to define the path of the aircraft are determined and the aircraft and engine performance can be evaluated as will be presented in the following sections.

This trajectory definition can easily be adapted and used for optimization procedures where the number of free parameters of the optimization problem will depend on the number of selected trajectory points and the chosen parameterization. In this

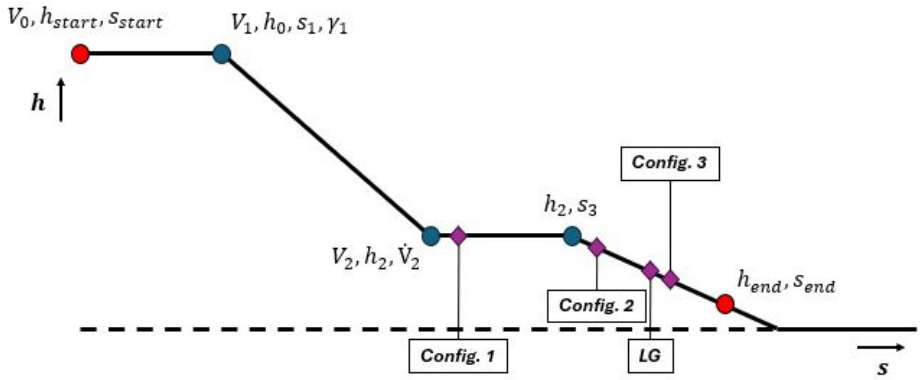

Figure 2.2: Sample trajectory definition for an approach procedure.

case, some constraints should also be considered in order to obtain viable procedures. These constraints concern safety requirements, operational limitations as well as path constrains. For example, for an arriving aircraft, during the final approach, the flight profile is restricted to level flight or descending segments with constant or decreasing speed, while for safety reasons and passenger comfortness, the descent angle should not exceed 5^o. Finally, a few speed constraints should be applied depending on the aircraft altitude and configuration.

This model has been used in Paper 2 to generate a number of noise abatement approach procedures and to perform an optimization on a conventional approach operation. More details, on the optimization constraints and speed limits can be found in the appended Paper 2. The trajectory definition has also been implemented in Paper 5 to generate the two procedures under examination.

2.3 Aircraft performance modelling and sizing

The aircraft performance is evaluated using the system of equations described by eq. 2.11, with the lift and drag defined as

$$L = \frac{1}{2}\rho V^2 C_L S_w \tag{2.13}$$

$$D = \frac{1}{2}\rho V^2 C_D S_w \tag{2.14}$$

where ρ is the density of the atmosphere, S_w, the reference wing area, and C_L and C_D, the lift and drag coefficients, respectively. The latter are functions of the angle of attack, flight Mach number and Reynolds number, and are usually not readily available.

Another method for the estimation of the lift and drag forces is through another common metric for the aerodynamic efficiency, namely, the lift-to-drag ratio, L/D. This metric varies with speed, aircraft configuration and angle of attack, and can be obtained either from aircraft models or from the Aircraft Noise and Performance database [39].

In this work, the latter approach was implemented. The aircraft that was used for the scenario studies is A321neo, mainly due to availability of data that facilitate the validation of the models. The aircraft is a narrow-body jet-airliner produced by Airbus that entered into service in May 2017. It is part of the A320neo family which is a development of the A320 family. Two engine options are available, CFM International LEAP and Pratt & Whitney PW1000G, leading to a $15\% - 20\%$ improvement in fuel efficiency compared to the A320 family. Key data for the aircraft are presented in Table 2.1.

Table 2.1: A321neo specifications [40], [41].

Length	44.51 m
Wingspan	35.80 m
Height	11.76 m
MTOW	97 t
Max. Payload	25.5 t
Fuel Capacity	32940 lt
Cruise Speed	0.78
Max. Speed	0.82
Typical Range	74000 km
Engines	2

For the lift-to-drag ratio, an available aircraft model was used for the A321-231, which has the same dimensions and similar characteristics to the aircraft of interest. It was, therefore, assumed that the lift-to-drag ratio for the two aircraft remains fairly similar. The assumed ratio together with the aircraft configurations are presented in Table 2.2. In the table, only the configurations that are commonly found during approach are presented. In general, the lift-to drag ratio varies with angle of attack. However, for the approach configurations, it was established from available FDR (Flight Data Recorder) data that the angle of attack varies only insignificantly within each configuration, with the maximum variation reaching 3.8 % which corresponds to a 0.5 % variation in lift-to-drag ratio. A constant average value for the lift-to-drag ratio was therefore assumed for every configuration.

Table 2.2: A321neo approach configuration settings [42] and lift-to-drag ratio from available model.

Configuration	Slats (^{o})	Flaps (^{o})	Landing gear	L/D
Clean	0	0	Up	17.76
1	18	0	Up	15.38
2	22	14	Up	12.45
			Down	9.35
3	22	21	Down	8.88
FULL	27	34	Down	8.32

2.4 Engine Performance Modeling and Conceptual Design

For the engine performance and conceptual design, already existing and verified tools developed at Chalmers were used, namely GESTPAN (GEneral Stationary and Transient Propulsion ANalysis) [43] and WEICO (WEight and COst estimation) [44]. GESTPAN is a generalized simulation tool that can perform design, off-design and transient analysis of gas turbine systems, while WEICO performs conceptual design and sizing by reading the engine performance files from GESTPAN and estimating the weight and geometric characteristics of the engine components for the selected design point.

During this thesis, these tools were used to develop a model for the A321neo with LEAP-1A engine configuration. The specific aircraft and engine were selected due to the availability of flight data and noise measurements that could be used for model validation. The engine of interest is a two-shaft, direct drive, high-bypass ratio turbofan. The engine includes a single stage fan, followed by a three-stage booster, a ten-stage high-pressure compressor, a two-stage high-pressure turbine and a seven-stage low-pressure turbine [45]. It incorporates a novel second-generation combustor type (Twin Annular Premixing Swirler) TAPS II resulting in a significant reduction in fuel consumption and emissions [46]. The LEAP-1A32 and LEAP-1A35A variants were used for the studies, with key performance parameters derived mainly from the ICAO emissions databank [47]. More details on the engine modelling and validation can be found in the appended Paper 1.

Chapter 3
Aircraft Noise Sources

3.1 Overview of aircraft noise

The noise generated from aircraft is due to a combination of the contributions of a number of sources of different nature. These sources can, generally, be classified as propulsive and non-propulsive. The former refer to all the sources that are related with the propulsion system, while the latter include all the airframe noise sources.

The relative contribution of each component depends on several factors, such as aircraft and engine technology and operational conditions. Historically, engine noise had been the dominant source. However, significant improvement has been achieved in engine noise mitigation with the introduction of high bypass ratio (BPR) engines and the incorporation of noise suppression mechanisms and noise reduction measures [48]–[50]. On the contrary, reduction in airframe noise has been proven more challenging, with limited changes on airframe design since the introduction of what is considered the first modern airliner, namely the Boeing 247, in 1933, as can be seen in Figure 3.1. This has lead to airframe noise becoming the dominant noise source in low engine power operating conditions with deployed high-lift devices and landing gears, e.g. during approach. This is in line with the trends that are presented in Figure 3.2, where it can be clearly observed that the reduction in departure noise is steeper. Another reason for this has been that the climb performance of aircraft has improved resulting in an increase in the distance between the aircraft and the ground and, therefore, in noise reduction [51]. For the final approach segment, this distance has not changed over the years.

Propulsive or engine noise involves all the components of the propulsion system. For a turbofan engine, that is, the fan, compressor, combustor, turbine and jet. An illustration of the relative contribution and directivity of these components is shown in Figure 3.3. The fan is the largest contributor in forward generated noise, while the compressor is of significantly less importance. In the engine exhaust, the fan and jet are the dominant sources with almost the same level of contribution but different directivity patterns. The turbine and the combustor contribute in the aft radiated noise but in a lower degree. This can, however, change as the fan and jet noise levels are continuously reduced. At this point, it is interesting to note that significant reduction has been achieved in jet noise level. In fact, the level shown

(a) Boeing 247 (first flight in 1933) [52].

(b) Airbus A321neo (first flight in 2016) [40].

Figure 3.1: First modern airliner and state-of-the-art aircraft.

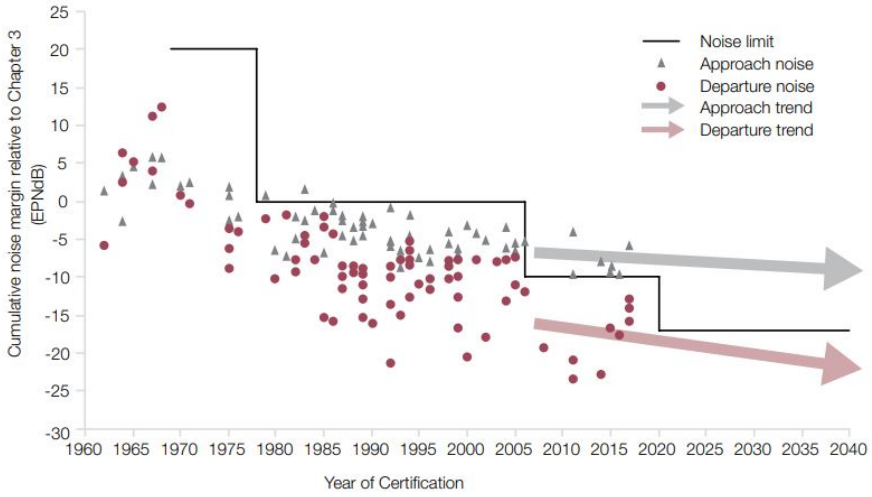

Figure 3.2: Trends in aircraft noise certification levels. Reprinted from *Airports Commission: final report* [12] under the Open Government License.

in Figure 3.3 is the result of the introduction of high BPR engines. In this type of engine, a significant portion of the inlet mass flow is diverted from the core of the engine, resulting in reduced jet exhaust velocities. Significant reduction has also been achieved in fan exhaust noise, mainly with the installation of acoustic lining [50]. This has also improved core noise and fan inlet noise but to a lesser degree.

Airframe noise can be defined as the noise that would be generated if the propulsion system was inoperative [48]. It is mainly created from turbulence in the flow over the surfaces and objects on the aircraft structure. The main sources of noise on the airframe are the trailing edges, such as the wing and tails, the high-lift devices, namely flaps and slats, and the landing gears. Depending on the structure, there can be more sources contributing more or less to the total airframe noise. These can be, for example, landing gear cavities [54] or wing cavities from the fuel over-pressure ports [55]. Although airframe noise is not of significant importance during most parts of the flight, due to either engine noise dominance or increased distance to the ground, it is becoming a dominant source during the final approach and landing,

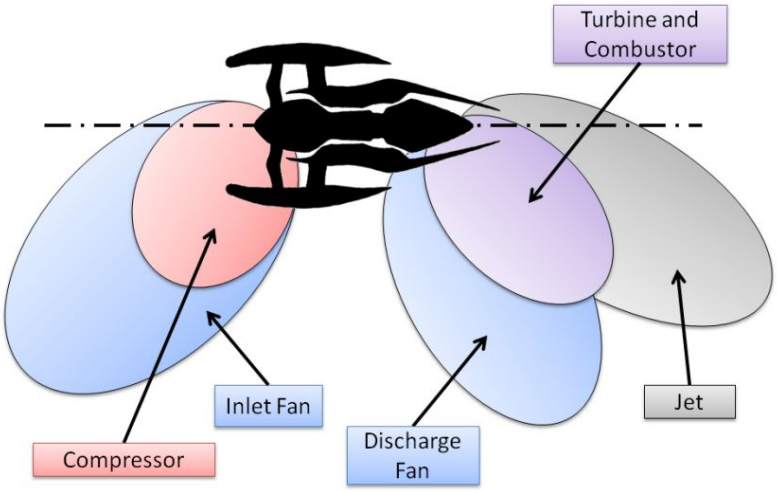

Figure 3.3: Noise contribution and directivity of high bypass ratio turbofan engine components. Reprinted from [53].

as the propulsive noise is continuously reduced. It also sets a potential lower noise barrier in the sense that even if aircraft engines become quite, airframe noise will still be present. Research and interest on airframe noise reduction has, therefore, increased the past few decades [56]–[58], and although some progress has been made, for example, the development of landing gear fairings, there are still obstacles that need to be overcome so as not to worsen the aerodynamic performance or interfere with maintenance procedures [56].

3.2 Noise prediction methods

Each of the aircraft noise sources described in the previous section generates noise due to one or more underlying mechanisms which will be described in the sections to follow. Several of these mechanisms can be identified on an aircraft causing sound of varying spectral characteristics and directivity, although the resulting noise spectra from each of these can be broadly categorized as broadband or tonal noise. The former is a type of noise whose energy is distributed over a broad range of frequencies and is usually caused by pressure fluctuations due to turbulent flow while the latter is a discrete frequency noise created by the rotating parts of the engine or by cavities and coves on or between the airframe structures. Which type of noise and source will be dominating in the total aircraft noise depends on various factors, such as aircraft and engine technology, operating conditions and weather conditions.

Methods and tools for predicting aircraft noise are often based on fully numerical approaches, such as computational fluid dynamics (CFD) and computational aeroacoustics (CAA) codes, or CFD coupled with application of the acoustic analogy [58], [59]. However, when the total aircraft noise is of interest, these approaches can be very computationally expensive and their implementation in noise prediction codes for system level studies and flight procedure evaluation is not practical. Therefore,

faster approaches are required, which can be separated into the following three categories [11], [58]–[60]:

- Analytical or physics-based methods: These are high fidelity methods based on physical laws of acoustics, fluid mechanics and thermodynamics, where the source noise is modelled as a combination of monopoles, dipoles, and quadrupoles. They are very flexible and can predict the noise from most scenarios with good accuracy. However, they are still computationally expensive and require very detailed input which is often not available. Thus, they are often combined with other approaches, such as CFD or with empirical data. Such an implementation is SIMUL [60], which separates the major sound sources and models the sound as a combination of physical laws and empirical methods.

- Semi-empirical models: They rely on simplifications of the physical laws and are developed based on databases. They require less input than the physics-based methods and provide sufficiently accurate estimations in most cases. Unfortunately, their accuracy is dependent on the database they were developed from. However, if revised and updated for newer aircraft types and engines, these methods can even be used to evaluate unconventional configurations. The most widely known tools in this category are ANOPP (Aircraft NOise Prediction Program) [61] and PANAM (Parametric Aircraft Noise Analysis Module) [62] which are well documented in the literature and have been used in many studies [63]–[66]. ANOPP has been the base for NASA's next generation noise prediction program, ANOPP2 [67], which combines semi-empirical with physics-based methods.

- Integrated or best practice methods: These are based on fully empirical correlations that are derived from databases and usually consider the aircraft as a whole. They are able to provide a good estimation for long-term averages and are used by several airports and national authorities. However, they do not provide any information about the individual component contribution to the total noise. The more commonly used methods and tools in this category are the ECACdoc29 [68] and the FAA's (Federal Aviation Authority) INM (Integrated Noise Model) [69] and AEDT (Aviation Environmental Design Tool) [70].

In this work, the noise estimation is based on empirical and semi-empirical noise source models found in the public literature. Their implementation was included in an open-source framework, CHOICE (Chalmers nOIse CodE), which is available on GitHub [71]. The basic outline of CHOICE is presented in Figure 3.4. The prediction starts by defining a trajectory and selecting an aircraft and engine. The inputs required for the noise calculation are then determined using the methods described in Chapter 2. The total SPL (Sound Pressure Level) is computed for every frequency and longitudinal directivity as the sum of the individual components for every point along the given trajectory. Propagation effects for a standard atmosphere are then

included and the SPL matrix at the microphone is estimated. This can be converted to EPNL (Effective Perceived Noise Level) in order to allow for comparison with the standard certification procedure [9] or it can be used to generate noise contours and auralizations.

The rest of this chapter is dedicated to the introduction of the implemented models and the underlying noise generation mechanisms for each component. The propagation effects will be discussed in the next chapter.

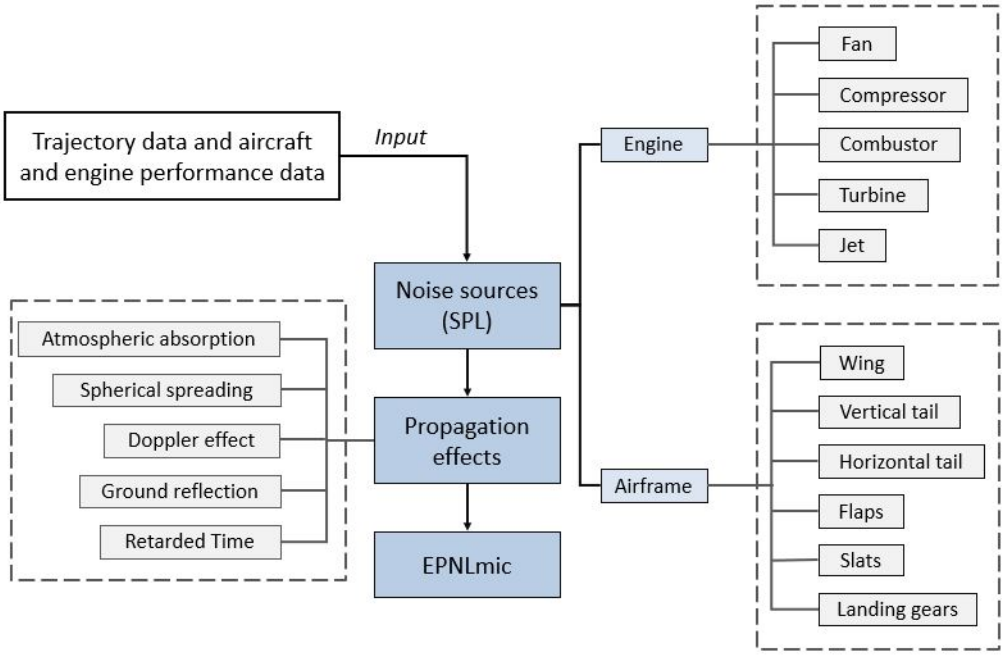

Figure 3.4: Flowchart of CHOICE.

3.2.1 Engine noise

Fan and compressor noise

The noise generated from the fan controls the total aircraft noise in most flight conditions. It is the largest engine noise contributor during final approach and dominates together with the jet at take-off [72]. At subsonic blade tip speeds, broadband fan noise is generated from random unsteady fluctuations due to turbulence in the flow passing the blades. This unsteadiness can be caused by turbulence in the wall and blade boundary layers, in the blade wakes and vortices, or in the freestream inlet flow [72], [73]. Tonal noise is caused by periodic lift fluctuations due to inlet flow turbulence or interaction between rotors and stators. Tones are generated at integer multiples of the blade-passing-frequency (BPF harmonics). At supersonic tip speeds, shocks are created at the rotor leading edge causing the generation of multiple pure tones, "buzz saw" noise, at multiples of the shaft rotational frequency. This phenomenon is usually observed during take-off.

The model used for the prediction of noise from the fan and the compressor components is based on the method introduced by Heidmann [73] and later updated by Kontos et al. [74]. According to this method, fan or compressor noise at the inlet duct is a combination of broadband, discrete-tone and, possibly, multiple pure tone noise. At the discharge duct, only fan broadband and discrete tone noise are present. The predicted noise is in 1/3 octave band frequencies of the free field noise pattern and the required parameters for the prediction are the mass flow rate, the total temperature rise for a fan or compressor stage and the design and operating point values of the rotor tip relative inlet Mach number.

The peak characteristic sound pressure level for all noise components, except the combination tone noise, is described by the following equation

$$L_c = 20\log\left(\frac{\Delta T}{\Delta T_0}\right) + 10\log\left(\frac{\dot{m}}{\dot{m}_0}\right) + F_1(M_{trd}, M_{tr}) + F_2(RSS) + F_3(\theta) \tag{3.1}$$

where $\Delta T/\Delta T_0$ is the temperature rise across the fan or compressor stage, normalized by a reference value, $\dot{m}/\dot{m}_0$ is the mass flow rate through the component over a reference mass flow rate, M_{trd} and M_{tr} are the rotor tip relative inlet Mach number at design and operating point, RSS is the rotor-stator spacing and θ is the angle between the observer and the engine inlet or the directivity angle. The values for F_1, F_2 and F_3 are taken from graphs provided in [73] and [74] and vary for every component.

Then, the sound pressure level spectrum for inlet and discharge broadband and discharge discrete tone noise is obtained from

$$SPL(f) = L_c + F_4(f/f_b) \tag{3.2}$$

while for inlet discrete tone noise from

$$SPL(f) = L_c + 10\log\left(10^{0.1F_4\left(\frac{f}{f_b}\right)} + 10^{0.1F_5\left(\frac{f}{f_b}\right)}\right) \tag{3.3}$$

where F_4 and F_5 are represented by functions provided in the reports and they differ for each component.

For the combination tone noise, the characteristic peak level at center frequencies one-half, one-fourth and one-eighth of the fundamental blade passage frequency is given by

$$L_c = 20\log\left(\frac{\Delta T}{\Delta T_0}\right) + 10\log\left(\frac{\dot{m}}{\dot{m}_0}\right) + F_1(M_{tr}) + F_2(\theta) + C \tag{3.4}$$

where F_1 and F_2 are provided in figures and C equals -5 dB for a fan with inlet guide vanes and 0 dB for a fan without inlet guide vanes. The sound pressure level spectrum for each of the three combination tone components is obtained from

$$SPL(f) = L_c + F_3(f/f_b) \tag{3.5}$$

where F_3 is provided in the relevant figure in the report.

The total combination tone noise sound pressure level spectrum is obtained by summing the spectrum of each of the three components on an energy basis.

Combustor noise

Although, not one of the dominant sources, the combustor has a strong contribution to the total engine noise especially in the low- and mid-frequency region. It is created by two distinct mechanisms, namely direct and indirect combustion noise [75]. The direct noise is associated with the combustion process itself as it is caused by heat fluctuations from the chemical reaction. The indirect noise is caused by pressure waves created from the temperature and velocity fluctuations of the hot gas as it convects the turbine stages [58], [76], [77].

The combustor noise source model was based on the model described by Gliebe et al. [77], [78] for low-emissions combustors. Farfield noise data were collected and analyzed for both SAC (Single-Annular Combustor) and DAC (Dual-Annular Combustor) and two separate correlations were developed taking into account the combustor geometry, cycle conditions, spectral frequency content and directivity.

Single-annular combustor: The spectral noise peaks for single-annular combustors are observed in three frequencies and directivities: 63, 160 and 630 Hz and 150^o, 130^o and 130^o, respectively. The procedure to calculate the overall sound pressure level starts from computing the normalized OASPL (Overall Sound Pressure Level) for every spectral peak.

$$OASPLN = a_3\theta_n^3 + a_2\theta_n^2 + a_1\theta_n + a_0, \tag{3.6}$$

where θ_n is the normalized directivity angle calculated from the peak angle as $\theta_n = \theta/\theta_p$ and the coefficients a_i are defined separately for each spectral peak [77].

The OASPL is, then, computed for every peak frequency as

$$OASPL(\theta) = OASPLN + OASPL(\theta_p) + b\,(SPL(F_C) - SPL(T_L)) \tag{3.7}$$

where b is a coefficient depending on the spectral peak and $SPL(F_C)$ and $SPL(T_L)$ are the combustor flow and turbine nozzle transmission-loss related effects which can be calculated as a function of the combustor performance parameters, the combustor dimensions, the number of ignited fuel nozzles and the turbine exit performance parameters. All functions and coefficients can be found in [77].

The peak overall sound pressure level from eq. 3.7 is computed as

$$OASPL(\theta_p) = -20\log(R_o) + H_{CP}\left(\frac{30}{N_f}\right)^c \tag{3.8}$$

where H_{CP} is a function of the cycle parameter, CP, [77], R_o is the observation radius which in the report is assumed equal to $150ft$, N_f is the number of ignited nozzles and c is a coefficient depending on the spectral peak.

The spectral shapes are computed from the normalized sound pressure level which is a function of normalized frequency and can be calculated as

$$SPLN(f_n) = k_0 + k_1 f_n - k_2 f_n^2 \tag{3.9}$$

where k_i are constants that are defined separately for each spectral peak [77].

Finally, the spectrum is determined for every frequency and directivity as

$$SPL(\theta, f) = OASPL(\theta) + SPLN(f_n) + a_{ft}\frac{(R_o - 3.281)}{1000} + 20\log\left(\frac{R_o}{3.281}\right) \quad (3.10)$$

where a_{ft} is the air attenuation factor in dB per $1000ft$. The last two terms are included to compute the source SPL at 1 m (or 3.281 ft) radius.

Dual-annular combustor: Dual-annular combustors were found to peak at two frequencies, 160 and 500 Hz, with one peak observer angle at 130^o. The basic equations are the same as presented in eqs. 3.6, 3.7, 3.9, 3.10 for the single annular combustor, though the coefficients, transmission-loss effects, cycle parameter and eq. 3.8 differ. The overall sound pressure level for every peak angle, in this case, is a function of the fuel-nozzles staging pattern and is defined as

$$OASPL(\theta_p) = K_{NF}\left(-20\log(R_o) + H_{CP}\left(\frac{20 + N_f}{N_{f,max}}\right)^{-X_K}\left(\frac{30}{20 + N_f}\right)^{M_f}\right) \quad (3.11)$$

where M_f varies for every peak frequency and the parameters K_{NF} and X_K vary with spectral peak frequency and fuel nozzle firing pattern and can be obtained from the relevant table in [77].

Turbine noise

Turbine noise is generally assumed to be a combination of broadband and discrete tone noise, generated from mechanisms similar to those of fan noise generation [58], [79]. More specifically, tonal noise is expected to arise from interaction between the rotors and stators, while broadband noise is caused by random lift fluctuations on the rotor and stator stages due to turbulent flow.

In this work, the method of Dunn and Peart [80] was implemented for predicting the turbine noise. The resultant spectra for both the broadband and the discrete tone noise are normalized with respect to the fundamental blade passage frequency of the last stage of the turbine and are given in 1/3 octave band levels at the free-field, index ($R = 1m$) conditions.

The broadband noise component for the peak 1/3 octave band level at a radius of 45.7 m from the source is given by

$$L_0 \cong 10\log\left(\left(\frac{V_{TR}c_0}{V_0 c_L}\right)^3 \frac{\dot{m}}{\dot{m}_0}\right) + F_1(\theta) - 10 \quad (3.12)$$

where V_{TR} is the relative tip speed of last rotor of the turbine (0.7 times the tip speed is used if V_{TR} is unknown), V_0 is the reference velocity equal to 0.305 m/s, $\dot{m}$ is the primary mass flow, $\dot{m}_0$ is the reference mass flow equal to 0.4536 kg/s, c_L is the speed of sound at the turbine exit, θ is the directivity angle relative to the inlet axis and F_1 is given by the empirical curve in Figure 52 of reference [80]. Note that the convective amplification factor included in the equation in the reference [80] has been removed, as it is included later in the prediction.

The sound pressure level spectrum at 45.7 m from the source can be obtained from

$$SPL(f)\mid_{45.7m} \cong L_0 + F_2(f/f_0) \tag{3.13}$$

where $f_0 = B\omega/60$ is the fundamental blade passage frequency of the last stage of the turbine, B is the number of blades for the last rotor stage of the turbine, ω is the shaft speed in rpm and F_2 is provided in Figure 54 of reference [80].

Similarly, the discrete tone component at a radius of 45.7 m from the source is calculated by

$$L_0 \cong 10\log\left(\left(\frac{V_{TR}}{V_0}\right)^{0.6}\left(\frac{c_0}{c_L}\right)^3 \frac{\dot{m}}{\dot{m}_0}\left(\frac{c}{s}\right)\right) + F_1(\theta) + 56 + K \tag{3.14}$$

where c/s is the stator/rotor spacing and K is a correction factor for turbofans with a primary nozzle exit plane upstream of the secondary nozzle exit plane, i.e. the JT8D.

The tones are added to the broadband spectrum, computed by eq. 3.13, and the spectrum at a radius of 1 m is calculated as follows

$$SPL(f)\mid_{1m} = SPL(f)\mid_{45.7m} + 33.2 + \Delta dB(f) \tag{3.15}$$

where $\Delta dB(f)$ is obtained from Table 4 in reference [80].

Jet noise

The jet still remains one of the most significant sources in aircraft noise, even though its contribution has decreased significantly as the BPR of the engines has increased. The primary mechanism in jet noise generation is the mixing of the high-speed exhaust flow with the bypass flow and the surrounding air causing turbulence and pressure fluctuations that create acoustic waves [76], [81]. As BPR is increased, the jet exhaust velocity is reduced resulting in a decrease in noise.

Jet noise was modeled as presented by Russel [82]. This method can be used to estimate source noise both from circular and coaxial jets, and it is based on extensive test data. The sound pressure levels from the test data are curve fitted, as a function of frequency and directivity, using bicubic splines and a third order Taylor series. The component noise levels are then defined for all frequencies and longitudinal directivities.

The circular jet noise is calculated as a function of the jet velocity and jet total temperature. For the coaxial jet the jet state properties for an equivalent single stream jet with the same mass flow, energy flow and thrust as the coaxial jet are used. These properties are the equivalent jet velocity, the equivalent jet total temperature, the velocity ratio of the outer stream to the inner stream, the temperature ratio and the area ratio. The 1/3 octave band sound pressure level is calculated as the summation of four components

$$SPL(\theta,\eta) = \overline{OAPWL} + D(\theta) + F(\eta) + RSL(\theta,\eta) + k_1 + k_2 + k_3 \tag{3.16}$$

where $\overline{OAPWL}$ is the normalized overall power level, $D(\theta)$ the directivity index, $F(\eta)$ the power spectrum level and $RSL(\theta, \eta)$ the relative spectrum level. The parameters k_1, k_2 and k_3 are constants that depend on the size of the jet, the microphone distance, the ambient conditions and the ratio between the reference power level and the reference mean square pressure level. The frequency parameter, η, is used instead of the frequency and is defined as

$$\eta = 10 \log \left(\frac{f D_e}{V_e} \right) \tag{3.17}$$

where D_e is the equivalent diameter of the coaxial or circular jet and V_e the nozzle exit equivalent flow velocity.

The four components in eq. 3.16 are empirically defined as a function of flow state parameters on each point of a grid, which consists of seven directivity coordinate points, $\theta_c = 0^o, 30^o, 60^o, 90^o, 120^o, 150^o, 180^o$ and seven frequency parameter coordinate points, $\eta_c = -1.5, -1.0, -0.5, 0.0, 0.5, 1.0, 1.5$. More specifically, they are computed by multiplying and summing their corresponding derivative values, obtained from the relevant tables in reference [82], with the derivative multiplier values, X_j. The derivative multipliers vary from 8 for the circular jet to 36 for the coaxial jet. They are obtained from a least square fit Taylor series and can be defined according to Table III in the same report, accounting for the exit flow parameters, which are computed using the equivalent jet flow properties as follows

$$x_i = \log \left(\frac{a_i}{a_{ir}} \right) \tag{3.18}$$

where a_i is the i_{th} prediction parameter or equivalent jet state property and a_{ir} is the standard value for the i_{th} prediction parameter.

Finally, with the four components determined at the reference coordinate points, cubic splines are used to obtain them in all directivities and frequencies and the sound pressure level is calculated.

3.2.2 Airframe noise

Airframe noise is one of the dominant noise sources during approach and landing. It is generated from the interaction of the airflow with the structures on the aircraft, e.g. landing gear, wings, flaps, etc, and it is, therefore, highly dependent on the aircraft speed. It is mainly of broadband nature, but as research has shown [54]–[56], [83], tonal components may also be present. The latter are not modelled in the presented noise prediction code. The rest of the components are separated into two categories, namely trailing-edge and high-lift systems noise and landing gear noise.

Trailing-edge and high-lift systems noise

For an aircraft in Clean configuration, aerodynamic noise is generated from the convection of the turbulent boundary layer past the trailing edges of the wing and tail surfaces [58], [84], [85]. As the slats are extended, a noise increment is caused.

This is assumed to be created by three processes; trailing-edge noise from turbulent flow at the slat trailing edge, noise due to flow separation from actuators and tracks exposed to the high-speed airflow, and mixing of the slat wake with the boundary layer and turbulence of the wing upper-surface. Finally, with the extension of flaps, the flap panels are submerged in the turbulent flow created by the wing, causing the generation of noise from lift fluctuation.

In this work, the noise from the wings, tail surfaces and high-lift systems was modelled according to the method proposed by Fink [84], [86]. The overall sound pressure level for the wing and horizontal tail surfaces is calculated as

$$OASPL = 50\log\left(\frac{V}{51.44}\right) + 10\log\left(\frac{\delta b}{h^2}\cos^2(\phi)\cos^2\left(\frac{\theta}{2}\right)\right) + 101.3 \tag{3.19}$$

where $\delta = 0.37(S/b)(VS/b\nu)^{-0.2}$ is the boundary layer thickness, V is the aircraft's speed, b is the wing or tail span, h the altitude, S the wing or tail area, ν the kinematic viscocity, and ϕ and θ, the lateral and longitudinal directivity, respectively. When calculating the noise from the vertical tail, $\cos^2(\phi)$ is substituted with $\sin^2(\phi)$.

The above eq. 3.19 refers to aerodynamically clean sailplanes. For jet aircraft, 6 dB should be added for the prediction of noise from the wing. The spectral shape is, then, calculated using a semi-empirical equation for the normalized spectral density of trailing edge from externally blown flaps. This is rewritten in terms of the 1/3 octave band sound pressure level as

$$SPL = OASPL + 10\log\left(0.613\left(\frac{f}{f_{max}}\right)^4\left(\left(\frac{f}{f_{max}}\right)^{3/2} + 0.5\right)^{-4}\right) + \Delta SPL \tag{3.20}$$

$$\Delta SPL = -0.03\left(\frac{R}{152.4}\right)\left|\left(\frac{f}{f_{max}}\right) - 1\right|^{3/2} \tag{3.21}$$

with R the distance to the observer and $f_{max} = 0.1V/\delta$ the frequency for maximum wing trailing-edge noise.

Trailing-edge flap noise is modelled as an increment of the trailing edge noise and varies directly with the flap area and the sine squared of the flap deflection angle, inversely with the far-field distance squared and directly with the sixth power of the airspeed. The frequency of the spectrum is scaled as a Strouhal number calculated for the flap chord.

A simpler approach is used for the calculation of noise caused by the extension of leading-edge high-lift devices. For leading-edge slats, it is assumed that the total noise generated is 3 dB above the spectrum predicted for the clean wing, with an additional peak of equal amplitude at a frequency, f_{max}, calculated as before but for the slat chord.

The total noise is calculated by summing the noise from all components as uncorrelated sources. The predicted level is 3 dB above free-field and, therefore, a 3 dB reduction is applied to the total noise.

Landing gear noise

Landing gear noise is, typically, of broadband content and its main generation mechanisms are turbulent flow separation caused by the various bluff-body structures (struts, joints, tires, etc.) and the interaction of these turbulent wakes with other structures, such as the high-lift systems [11], [56], as they flow downstream. In both cases, the interaction causes a small part of the turbulence energy to transform into propagating acoustic waves. Tonal components may also arise, due to coherent vortex shedding off small structures, such as the wires and dressings, [56], [87] and cavities on the landing gear structure [54], [87], [88]. From these mechanisms, it is only the first phenomenon that is usually modelled in semi-empirical prediction methods [84], [89], [90] as it is considered to be the dominant source of landing gear noise.

The selected method for landing gear noise prediction was proposed by Sen et al. [89]. According to this method, the noise from the landing gear can be decomposed into four main components; low-frequency component which is generated by the struts, mid-frequency component caused by the hydraulic pipes near the break assembly, high-frequency component from the electric wire and small pipes, and tire noise component. The overall sound pressure level for all components is expressed through the same functional relationship as

$$OASPL_i = \Delta_i + 60\log\left(\frac{V_l}{c}\right) + 20\log\left(\frac{D_i\sin(\theta)}{R}\right) + 10\log(N_s N_t) \tag{3.22}$$

where i refers to each noise component, c to the local speed of sound, D_i to a respective length scale for each component, θ to the polar directivity, R to the distance to the observer, and N_s and N_t, to the number of main struts and tires. The local airspeed, V_l, can be determined as percentage of the aircraft airspeed, usually varying between 75 % to 83 % for conventional aircraft [90]–[92]. The constant, Δ_i, is defined separately for each component and can be found in [89].

The 1/3 octave band sound pressure level spectrum is, then, determined from the OASPL and a normalized SPL function of the Strouhal number as

$$SPL_i = OASPL_i + \Delta SPL(St_i) \tag{3.23}$$

with

$$St_i = \log\frac{fD_i}{V_l} \tag{3.24}$$

and

$$\Delta SPL(St_i) = x_{i0} + x_{i1}St_i + x_{i2}St_i^2 + x_{i3}St_i^3 + x_{i4}St_i^4 + x_{i5}St_i^5 + x_{i6}St_i^6 + x_{i7}St_i^7 \tag{3.25}$$

where the coefficients x_i depend on the component and can be found in Tables 4.2 through 4.5 in the report [89].

3.2.3 Limitations of the models

The source prediction methods for the fan and the turbine described in the previous sections result in a slight overprediction of the noise level in approach condition. This

can be attributed to several factors with the most dominant one being that both methods refer to hardwall prediction and no acoustic treatment is included. The effect of acoustic treatment becomes even more prominent as technology advances and since these methods were developed based on older engine models it is necessary to account for any noise reduction mechanisms. An example of the noise reduction in the fan and turbine components due to acoustic treatment is presented in Figure 3.5. The original figure can be found in the report by Owens [93] and later adapted by Groeneweg and Rice [72] in a report where a detailed discussion regarding fan noise generation and suppression and the mechanisms involved is provided. Further discussion on aircraft noise reduction technologies can be found in several review articles, such as the ones presented by Casalino et al. [94], Envia [95], Leylekian et al. [96] and Bertsch et al. [58].

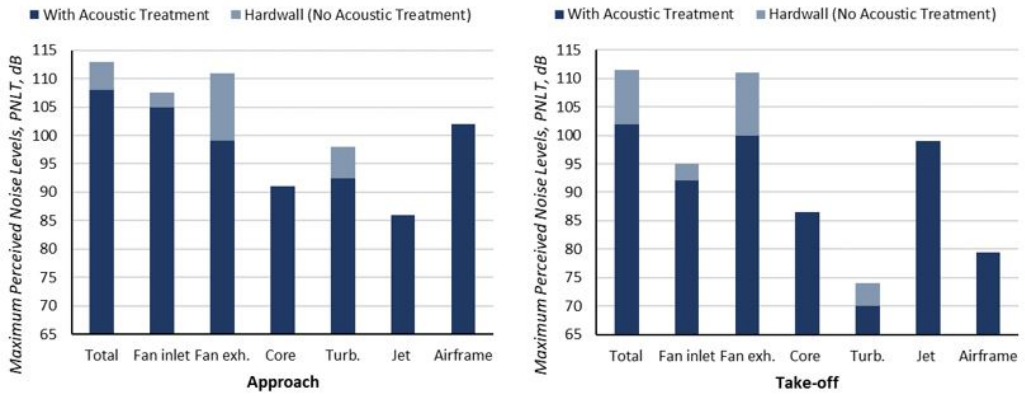

Figure 3.5: Effect of acoustic treatment on engine components. Figure reproduced from [93].

Regarding the fan noise, another possible reason for the overprediction is that the model was developed based on measurements from static fan tests. During such tests, ingestion of vortices or other turbulence from the test stand or other nearby structures can interfere with the data, as described by Krejsa and Stone [97]. Despite these shortcomings, that are common in most empirical models, the model developed by Heidmann [73] is still the most widely used. An attempt to provide an update for the method was performed by Krejsa and Stone [97]. However, as they state in the report, the method was developed based on data from one fan and further tests should be made to determine its prediction accuracy.

Prediction of turbine noise is generally less accurate than for other components. Existing turbine noise models do not provide very accurate estimations as predicted and measured levels tend to deviate by up to 9 dB [79]. This could partly be attributed to the fact that the turbine never works in isolation but is always dependent on the combustor [11], [98] and attempts in separating the two sources have not been fully successful [99]. Thus, clean and reliable experimental data are hard to find and prediction methods are usually developed by separating the measurement spectra in frequency regions [80] or with the help of CFD analysis and actuator disk theory [77]. An assessment of existing models with the purpose of selecting a recommended model and identifying turbine noise research requirements was performed by Krejsa

and Valerino [79]. They compared several semi-empirical turbine noise prediction methods with measurements and concluded that the most accurate prediction was provided by the Dunn and Peart method [80], that was introduced in Section 3.2.1. However, they found that even this method resulted in a significant deviation ranging from -6 to 8 dB, which is in line with the prediction tolerance that Dunn and Peart state in their report [80]. They suggested that further research is required to better understand the turbine noise generation mechanisms and that the method should be reevaluated and modified as more data become available. Following this comment, no further updates or more recent correlations have been found.

Combustor noise prediction is subject to uncertainties for the same reasons that were discussed in the previous paragraph, although, it is generally believed to be more accurate than the turbine noise prediction. Hultgren [100] performed a comparative assessment of existing noise models, mainly focusing on the models developed by Stone et al. [101] and the model used in ANOPP [102], [103]. The two models, generally, showed different spectral shapes and peak noise level and suggested modifications were proposed by the author for the ANOPP model, while some unclear issues of the Stone et al. model were highlighted, noting that it should only be used for General Electric turbofan engines. The implemented model [77], although mentioned in the study [100], was not assessed. At the present time, it is considered the best fit for the work described in this thesis as it is the only one, to the author's knowledge, that provides a prediction for dual-annular combustors. Whether the predictions are accurate or not is not possible to evaluate due to the low combustion noise level in the examined cases, although the general trend is well captured. However, since the relevant contribution of this component is expected to increase, as fan and jet noise trends continue to decrease, more research should be directed into understanding this component and developing accurate models [100] and, if needed, the present method should be updated.

Jet noise is considered to be one of the most well understood noise components [58] and most of the existing prediction models [82], [104], [105] seem to agree on its spectral shape. The selected method [82] has the advantage of treating the circular and coaxial jet together. Similarly to the case of the combustor, no issues or uncertainties can be identified at the present moment.

Research on airframe noise began in the 1970s when it was realized that it will determine the lower limit of total aircraft noise. Since then, a number of semi-empirical models have been developed starting with the prediction developed by Fink [84], which is still one of the most widely used methods and is also implemented in this work. This method provides a fairly good estimation and is easy to implement in noise prediction codes due to the simplified equations that do not require detailed geometric characteristics of the components. Unfortunately, these simplification may lead to inaccuracies in the spectral shapes and/or noise level. Slat noise, especially, is modelled as an increment to the total trailing edge noise, despite the complex noise generation mechanisms behind it [106]. Studies have shown that the spectral shape of the component depends on its geometric characteristics [106], [107]. There have been a number of more recent efforts to model the flap [89], [108]–[110] and slat noise [89], [110]–[112], which, however could not be implemented due to unspecified

or unclear parameters, as was also suggested by Filippone [11], or for the case of Brooks' and Humphreys' method [109] and Molin's method [110], due to the level of details required in the input, such as for example, the chordwise pressure coefficient distribution for the flap and wall pressure fluctuation spectrum, respectively. These methods [109], [110] are leaning towards the physics-based category of noise prediction. With regard to the landing gear noise, several methods were tested, [84], [89], [90], but the one developed by Sen et al. [89] was found to be the most straightforward and accurate (in comparison to the available noise measurement data). The drawback of the method, as with most available methods, is that only the broadband noise component is estimated and that there is no indication of the lateral directivity variation. Finally, several studies have been dedicated to noise reduction measures for airframe components [56], [81], [113]–[116], which are unfortunately hard to model with the implemented semi-empirical models.

The total noise prediction is based on the assumption that the noise sources are uncorrelated and are, therefore, acting independently. However, this assumption is not entirely true as there are a number of installation and interaction effects [58], depending on the operating conditions. These effects may include scattering, reflection, shielding and changes in the flow conditions around a component and may result in overall noise reduction, generation of additional sources or alternations in the directivity characteristics. For a typical aircraft-engine configuration, most sources will be affected more or less by these effects, but the sources located at the aft of the engine, mainly the jet, will experience the largest influence due to interaction with the wing and flaps. More specifically, the characteristics of jet noise are altered as the high frequency noise is affected by reflection of the jet mixing noise at the wing, and the low-frequency noise is increased due to scattering as the pressure waves pass the wing trailing edge [117]–[119]. During approach and the initial part of take-off, there are even more interaction effects, such as, between the jet exhaust flow and the flaps [117], [120], [121], but also the main landing gears and the flaps [122], [123]. Both these effects influence the flow conditions around the flaps, while in the case of the former, a "scrubbing" noise is also generated which, however, shows similar spectral characteristics to the trailing-edge noise and is not always distinguishable [117], [119]. Shielding effects are mainly relevant for over-the-wing engine installation [124], [125] or future aircraft concepts, such as the blended-wing-body [126], [127], where the propagating pressure field is disrupted by some obstacle. However, they can occur in some, although limited, cases in conventional aircraft depending on the position of the receiver and the state of the aircraft, e.g. shielding from the fuselage at low altitude or from banking, for an observer located at the side of the ground path. All these effects may alter the characteristics of the sound to a larger or lesser degree, but, unfortunately, they are not captured by the component methods implemented in this work.

3.2.4 Noise suppression

Considering the first two points of the previous section, namely the fan and turbine overprediction, a simple noise suppression module has been implemented, where a

suppression factor is set and applied for every frequency and directivity. The method was described by Wilson [128] and can be applied to any component but is mainly used for the fan inlet, fan discharge and turbine components. The implementation of the factor is described by the following equations.

$$\langle p^2 \rangle_S = \langle p^2 \rangle S \tag{3.26}$$

$$S = 10^{S_{dB}/10} \tag{3.27}$$

where S_{dB} is the desired suppression (negative value) in dB, S the suppression factor and $\langle p^2 \rangle$ and $\langle p^2 \rangle_S$ the unsuppressed and suppressed mean square acoustic pressure, respectively. Indicative values for the suppression can be found in the report by Willshire and Garber [63].

3.2.5 Lateral directivity and installation effects

The implemented semi-empirical models predict the source noise for every frequency and longitudinal directivity which is sufficient for noise prediction from flyover aircraft (directly above the observer). However, for generating noise contours over an area or for predicting the noise at an observer located at the side of the ground path, the lateral directivity is also required. For the engine components, one could assume that the generated sound intensity is equal in all radial directions, due to the engine symmetry, and, therefore, the lateral directivity would not lead to any change in the noise level. However, as mentioned in Section 3.2.3, there are several installation effects that might be present depending on the engine position and that could influence the lateral directivity of the engine components. The prediction of trailing-edge and high-lift systems noise includes an estimation of the lateral directivity which indicates a decreasing noise trend as the observer is moving towards the side of the aircraft, while no information is given for the lateral directivity of the landing gear.

It is generally agreed that the lateral directivity of the aircraft is mainly attributed to the engine installation effects [68], [129]–[133] and varies depending on the aircraft-engine configuration, i.e. wing-mounted engine or fuselage mounted engine. Several empirical correlations have been proposed to model these effects [129]–[133] which, generally, indicate some differences. These could be attributed to the fact that for receiver positions where the lateral directivity becomes important, there are more uncertainties in the noise measurements as the aircraft either has to be closer to the ground or the source-receiver distance has to be larger [132]. For the work presented in this thesis, the method proposed in the standards SAE AIR 5662 [133] and ECAC Doc29 [68] was chosen to model the lateral directivity as it is the most general (not aircraft specific) and it was the most straightforward to implement. This method was compared with other models and measurements by Krebs et al. [130] and Wunderli et al. [132]. In some cases, mainly when the aircraft directivity pattern was less pronounced, a relatively good agreement was observed between the SAE model and their proposed method and measurements, while more significant deviations were found for aircraft with stronger directivity patterns. At the moment, the proposed

methodology from SAE AIR 5662 is considered the best fit, noting that it should be updated if more accurate methods become available.

According to the proposed method, the sound level at the side of the aircraft can be modelled as

$$L_{lateral} = L_{under} + E_{Eng}(\phi) \tag{3.28}$$

with

$$E_{Eng}(\phi) = \begin{cases} 10\log\left(0.1225\cos^2(\phi) + \sin^2(\phi)\right)^{0.329}, & \text{fuselage-mounted engine} \\ 10\log\left(\frac{(0.0039\cos^2(\phi)+\sin^2(\phi))^{0.062}}{0.8786\sin^2(2\phi)+\cos^2(2\phi)}\right), & \text{wing-mounted engine} \\ 0, & \text{propeller-driven aircraft} \end{cases} \tag{3.29}$$

where $L_{lateral}$ and L_{under} is the sound level at the side and under the aircraft, respectively, $E_{Eng}(\phi)$ is the engine installation effect and ϕ is the depression angle.

It should be noted that the methodology described in SAE AIR 5662 models the total lateral attenuation experienced by an observer on the ground. It, therefore, includes more effects such as the ground surface absorption and refraction and scattering due to wind and other meteorological. In this work, only the empirical formula for the engine installation effects is considered and the attenuation due to ground reflection and atmospheric effects is modelled separately through more detailed methods that are described in the next chapter of the thesis.

3.2.6 Total aircraft noise

The total noise emitted from the aircraft is computed as the sum of all the uncorrelated sources, assuming that the aircraft is acting as a point source. All the models predict the noise at one meter radius and, therefore, the total noise is also calculated at a unit sphere. The summation is performed on an energy basis as

$$SPL_{total} = 10\log\sum_{i=1}^{i=N_{sources}} 10^{SPL_i/10} \tag{3.30}$$

where $N_{sources}$ is the number of sources and SPL_i is the predicted sound pressure level for each source.

Before summing the components, engine noise sources are corrected to account for the number of engines on the aircraft. This is performed by summing incoherently the predicted source noise level for every engine component according to the number of engines.

A detailed comparison of the total source noise prediction with flyover noise measurements for approach conditions has been performed in Paper 3.

Chapter 4
Sound Propagation

The noise received by the microphone or an observer on the ground is subject to several effects, which can be broadly separated into kinematic or moving source effects and atmospheric propagation effects. The former refer to effects that are dependent on the source motion. These are the retarded time, convective amplification and Doppler shift. As the sound travels through the atmosphere, there are several other effects that impact its characteristics before it reaches the observer. These effects include atmospheric absorption, spherical spreading, change in atmospheric characteristic impedance, and ground reflection.

4.1 Source motion effects

The motion of the aircraft causes an alternation in the characteristics of the generated noise. The sound that is heard by a static observer will be different in both frequency and amplitude, even if no other atmospheric effects are present. The change in frequency is known as the Doppler effect, while the amplitude variation is caused by convective amplification. The former is a well known effect and states that the frequency of a wave reaching an observer standing still will be shifted compared to the emitted frequency from a moving source. The frequency received by the observer is calculated by

$$f_{observer} = \frac{f_{source}}{1 - M\cos(\theta)} \tag{4.1}$$

where θ is the angle between the flight velocity and the direction of sound propagation to the observer.

Convective amplification refers to source and propagation effects associated with the source motion. It is an important factor to consider for realistic noise prediction of in-flight conditions as most of the empirical noise prediction methods refer to static conditions. The mean square acoustic pressure, accounting for this effect, is modified as follows

$$p^2 = \frac{p_s^2}{(1 - M\cos(\theta))^4} \tag{4.2}$$

where p_s^2 is the mean square pressure in static conditions as predicted by the empirical models.

The convective amplification factor (denominator in eq. 4.2) depends on the nature of the source [134], but for most noise sources found on aircraft eq. 4.2 is a good approximation [61], [129], [135].

The motion of the aircraft causes another effect which is best illustrated with a sketch as presented in Figure 4.1. Assuming a simple scenario where the sound travels in a straight line path and there are no reflections, the sound emitted at a time t_e from a distance R_e will reach the observer at a time t_o when the aircraft has moved to a distance R_o. The time required for the sound to travel between the aircraft and the observer will be R_e/c, where c is the speed of sound. Hence, the sound will reach the observer at $t_o = t_e + R_e/c$. The time, t_e that the source emitted the observed sound is called emission or retarded time.

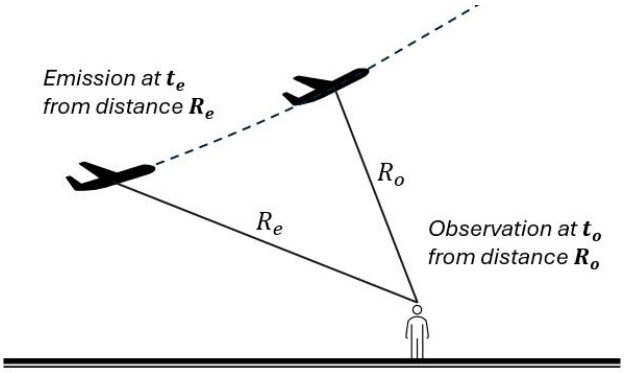

Figure 4.1: Retarded time effect for a moving source.

4.2 Atmospheric propagation effects

4.2.1 Spherical spreading

Spherical spreading describes the phenomenon of uniform wave propagation away from a point source in all directions. If the emitted acoustic power from the source is equal in all directions, its distribution must remain constant over any sphere around the source. Therefore, the power transmitted per unit area, i.e. the acoustic intensity, decreases proportionally with $1/R^2$, where R is the radius of the sphere and the area of the sphere increases with R^2. Hence, the noise received by an observer on the ground is highly dependent on the distance between the aircraft and the observer.

4.2.2 Atmospheric absorption

An emitted sound wave from an aircraft travels through the atmosphere causing its magnitude to decrease due to three main mechanisms. The first mechanism is the classical absorption which is a result of energy dissipation due to viscous losses and heat conduction. The second and third mechanism are both referred as molecular

absorption. One is caused by rotational relaxation and the other by vibrational relaxation processes of oxygen and nitrogen. These terms are modelled according to the ISO 9613-1:1993 standard [136] as

$$\begin{aligned}
&\alpha(f) \\
&= \alpha_{cl} + \alpha_{mol} + \alpha_{vib,O} + \alpha_{vib,N} \\
&= 8.686 f^2 \left(1.84\ 10^{-11}\ \frac{p_0}{p_s} \left(\frac{T}{T_0} \right)^{1/2} \right. \\
&\quad \left. + \left(\frac{T}{T_0} \right)^{-5/2} \left(0.01275\, e^{\frac{-2239.1}{T}} \left(f_{rO} + \frac{f^2}{f_{rO}} \right)^{-1} + 0.1068\, e^{\frac{-3352.0}{T}} \left(f_{rN} + \frac{f^2}{f_{rN}} \right)^{-1} \right) \right)
\end{aligned} \tag{4.3}$$

where f is the frequency, p_s and T the atmospheric static pressure and temperature, and p_0 and T_0 the reference ambient pressure and temperature, respectively. The oxygen and nitrogen relaxation frequencies, f_{rO} and f_{rN}, can be determined as a function of ambient atmospheric conditions and relative humidity.

4.2.3 Ground reflection

Ground reflection occurs when the sound waves from a source to an observer are not travelling directly but instead are reflected on the ground and can either enhance or diminish the observed sound intensity, depending on the phase difference between the received waves. The amount of attenuation of the incident to the ground wave is dependent on the ground surface type, which can vary from a soft surface, such as snow, to a hard surface, such as asphalt. The surface characteristics can, generally, be described through a parameter called acoustic impedance, which is an indicator of the amount of opposition of a surface or material to an acoustic flow.

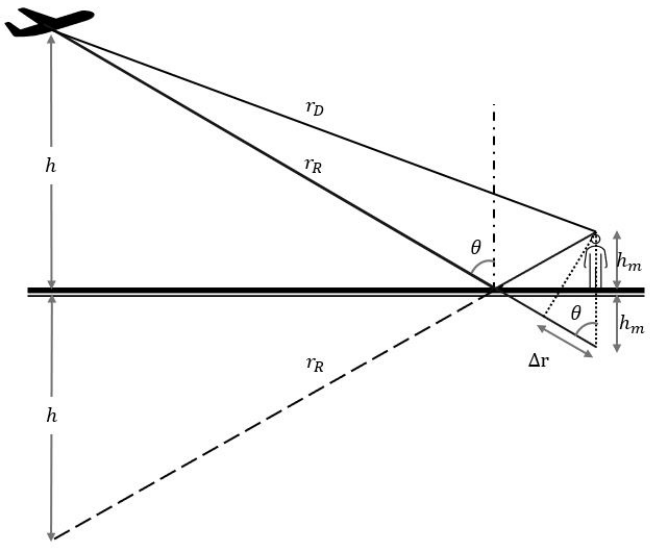

Figure 4.2: Ground reflection of sound ray.

The concept of ground reflection for rectilinear (straight line) propagation is presented in Figure 4.2. Modelling of this effect is based on the method presented by Zorumski [61]. This method is based on the Chien-Soroka [137] theory which assumes that the ground is a locally reacting uniform plane and that the aircraft is a point source. Because the predicted noise from the semi-empirical models is in 1/3 octave band representation, a division in sub-bands is required in order to predict the ground effect with more accuracy. Thus, each 1/3 octave band is divided into $N_b = 2m + 1$ sub-bands, where m is an integer number. The mean square acoustic pressure, with the ground effect included, is calculated by

$$\langle p^2 \rangle_{gr} = \langle p^2 \rangle_{ff} G = \langle p^2 \rangle_{ff} \left(1 + R^2 + 2RC \cos\left(a + k\Delta r\right) \frac{\sin((K-1)k\Delta r)}{(K-1)k\Delta r} \right) \quad (4.4)$$

where $\langle p^2 \rangle_{ff}$ is the free-field mean square acoustic pressure and G represents the ground-effects factor. $K = 2^{1/(6N_b)}$ is a sub-band correction factor and C is the coherence coefficient, which indicates the portion of the initial acoustic energy in which phase relation is maintained. k is the wave number and $\Delta r = 2h_m \cos(\theta)$ the path-length difference, as presented in Figure 4.2. Finally, R and α are the magnitude and argument of the complex spherical-wave reflection coefficient, which is computed as

$$Re^{ja} = \Gamma + (1 - \Gamma)F \quad (4.5)$$

with F the ground wave function and Γ the plane wave reflection coefficient which is calculated as a function of the ground impedance. The latter is predicted according to the recommended method by Delany and Bazley [138] who developed an empirical relationship as a function of frequency and flow resistivity. Flow resistivity is defined as the airflow resistance of a surface. In general, the higher the resistivity, the less the sound wave is absorbed. Typical values of the flow resistivity can be found in [139].

4.3 Noise metrics

When computing the noise from an aircraft on the ground there are several metrics that can be used depending on the application or purpose of the prediction. For comparison with noise certification levels, as defined by ICAO [9], the effective perceived noise level ($EPNL$) is commonly used, while for comparison with measurements from flyover aircraft, sound pressure level (SPL or L_p) or A-weighted sound pressure level (L_{pA}) is usually preferred. Noise mapping is usually performed using the sound exposure level (SEL) or in some cases the maximum A-weighted sound pressure level (L_{Amax}). A quick overview of these metrics is presented below. It should be noted that these are not the only available noise metrics, but the description is limited to the ones that have been used in the studies that are part of this thesis.

4.3.1 Effective perceived noise level

The $EPNL$ is a metric that accounts for the human perception of the spectral characteristics and duration of the sound. It is used for single aircraft events at a

single measurement point, usually certification point, and it is expressed in $EPNdB$. $EPNL$ cannot be measured directly, instead it is computed from the perceived noise level (PNL) by applying a correction for spectral irregularities (tonal components) and the duration of the sound [140]. The latter is computed from measured or predicted SPL by applying a frequency dependent weighting factor that can be obtained from curves.

4.3.2 Maximum A-weighted sound pressure level

L_{Amax} is simply the maximum A-weighted sound pressure level (in $dB(A)$) during a specified period, where A-weighting is a frequency dependent curve that can be applied on the SPL to account for the relative loudness as perceived by the human ear. Because it only provides a measure of the instantaneous noise level and does not account for the cumulative exposure, it is usually used together with other metrics, such as the sound exposure level.

4.3.3 Sound exposure level

The SEL is a metric that represents the cumulative sound energy of an event, taking into consideration both the noise level experienced and the duration of exposure. It is expressed in dB or $dB(A)$ and indicates the equivalent sound energy that would be produced in one second. It is a good metric for comparison of individual aircraft noise events with different duration. It can be calculated by integrating the sound pressure squared over reference pressure squared for the specified period.

Chapter 5
Aircraft Noise Synthesis

5.1 The concept of auralization

Auralization is the process of generating audible sound from numerical data [141]. It can be considered as equivalent to visualization but for acoustic phenomena. A tool like that can be very useful as it provides a means to communicate noise related scientific findings to the general public but also a way for the general public to contribute to research through subjective assessment of the noise impact of different scenarios. In the aviation sector, specifically, it can be used to facilitate the decision-making process during procedure design or during the development and design of new engine and aircraft concepts.

The auralization process revolves around three basic elements; source prediction, sound propagation and sound reproduction (or synthesis) through signal processing [141], [142]. The order of the last two can be interchangeable with the synthesis performed either before or after the propagation. In the former case, the propagation is performed in the time domain while in the latter in the frequency domain. A detailed description of the two approaches was presented by Rizzi and Sahai [142].

The models required for the sound source prediction and propagation have been described in the previous sections. This section concerns the third element in the auralization process, namely the signal processing and synthesis. In the subsections to follow, a short introduction to signal processing is provided where some basic concepts and methods are explained, followed by a description of the synthesis methodology.

5.2 Signal processing

5.2.1 Fourier transform

The Fourier Transform is one of the most useful techniques in signal processing, as it allows to move from the time to the frequency domain, and vice versa (Inverse Fourier Transform). It can be applied to any periodic or non-periodic signal (a function of time), transforming it into an alternate frequency domain representation,

written as the sum of simple sinusoidal waves of various frequencies. The Fourier transform is defined as

$$X(f) = \int_{-\infty}^{\infty} x(t)e^{-j2\pi ft}dt \tag{5.1}$$

where $X(f)$ is a two-sided complex continuous spectrum and $x(t)$ is a time domain signal.

The inverse operation can be used to obtain the original signal as

$$x(t) = \int_{-\infty}^{\infty} X(f)e^{j2\pi ft}df \tag{5.2}$$

In digital applications, only a finite number of sample points is available. In order to obtain an adequate representation of the signal, the sampling rate should be at least double the frequency of the highest frequency found in the signal. This sampling rate is called Nyquist frequency. Assuming that this condition is fulfilled, a discretised version of the Fourier transform should be applied on the signal to obtain the frequency domain representation. This is called the Discrete Fourier Transform (DFT) and is defined as

$$X(k) = \sum_{n=0}^{N-1} x(n)e^{-j2\pi kn/N},\ k = 0, 1, ..., N-1 \tag{5.3}$$

where k is the frequency index, n is the signal sample number and N is the total number of samples.

Similarly, the inverse transform, namely Inverse Discrete Fourier Transform (IDFT), can be determined from the following equation

$$x(n) = \frac{1}{N}\sum_{k=0}^{N-1} X(k)e^{j2\pi kn/N},\ n = 0, 1, ..., N-1 \tag{5.4}$$

An optimized version of the DFT is often used in acoustic signal processing, namely the Fast Fourier Transform (FFT), which is a more efficient and faster implementation of the DFT. There are various FFT algorithms but the oldest and most commonly used is the Cooley and Tukey algorithm [143] that divides a DFT of size N into N_1 smaller DFTs of size N_2, where $N = N_1N_2$. Finally, it is worth noting that if it is desired to increase the frequency resolution of a signal's spectrum, it is possible to do that by simply zero-padding the signal (adding zeros until the desired length is reached) before the FFT is applied [144], [145].

5.2.2 Digital filters

Filters are commonly used in signal processing to modify the characteristics of a signal in a desired manner [143]. The basic idea behind a filter is illustrated in Figure 5.1.

A filter is usually characterized by its transfer function, meaning a function that describes the relation between the input and output of the system. If $X(f)$ and $Y(f)$

Figure 5.1: Block diagram of a digital filter.

are the Fourier transforms of the input signal, $x(t)$, and output signal, $y(t)$, the filter transfer function for a linear time-invariant system can be defined as

$$H(f) = \frac{Y(f)}{X(f)} \tag{5.5}$$

Digital filters can generally be divided into infinite impulse response (IIR) and finite impulse response (FIR) filters. Breaking down these terms, the impulse response of a filter is the response or output of the filter when the input is a unit impulse at $t = 0$. That said, an IIR filter is one whose impulse response never reaches zero, i.e. is of infinite duration, because the filter output depends not only on the present and past inputs but also on recursive terms (past outputs). On the contrary, an FIR filter is a non-recursive filter with an impulse response of finite duration.

For real time applications, the filters must be causal, meaning that the output will only depend on present and past samples [144]. A non-causal filter will also require future samples as input and therefore is not suitable to operate in real-time. A causal filter can be designed from a non-causal impulse response by simply shifting it in the time domain and truncating it to the desired length. This process causes a delay which should be compensated in the final signal.

In this work, causal FIR filters are used to represent the sound propagation models for atmospheric absorption and ground reflection. The transfer functions of the filters correspond to the ratio of the received and emitted signal. Because the propagation effects vary depending on the position of the aircraft, the filters are varied with time.

5.2.3 Convolution

Convolution is the mathematical operation that is used to apply a filter to a signal. It is, therefore, equivalent to filtering a signal. It is defined as the integral of the product of two signals after one is reversed and shifted and can be written as [141]:

$$y(t) = x(t) * h(t) = \int_{-\infty}^{\infty} x(\tau)h(t-\tau)\,d\tau \tag{5.6}$$

where $x(t)$ is the input signal that is filtered with $h(t)$. Note that the convolution operation is symbolized with $*$, just as addition is symbolized with $+$.

In digital signal processing, the signals are of finite length and the discrete form of the convolution is more useful. Eq. 5.6 is, therefore, rewritten as follows

$$y(n) = x(n) * h(n) = \sum_{m=0}^{N-1} x(m)h(n-m) \tag{5.7}$$

This is the operation that is illustrated by the block diagram in Figure 5.1. It should be noted here that if a signal of length N is convolved with a filter of length M, the output signal will have a total length equal to $N + M - 1$ [145].

There are generally two ways to perform the convolution operation. The classic procedure is done in the time domain and is represented by eq. 5.7, using FIR filters. It is the most direct way but can be computationally inefficient if the signals are long [144], [145]. The second more efficient way is in the frequency domain and is called FFT convolution as it makes use of the FFT algorithm. It is based on the principal that convolution in the time domain is equivalent to multiplication in the frequency domain. Therefore, the input signal is transformed to the frequency domain and multiplied with the transfer function of the filter before transformed back in the time domain.

5.2.4 Overlap-add method

When a signal is very long, it can be more efficient to divide it into smaller blocks of equal length and process the generated blocks using the desired operation. The processed blocks are then recombined to form the final signal. This technique is called overlap-add method, and is commonly used to evaluate the convolution of a long signal with an FIR filter.

Assuming that a signal, $x(n)$, of length N is to be filtered with a filter, $h(n)$ of length M, where N is much longer than M. The signal can, then, be divided into blocks of length L as illustrated in Figure 5.2. Each block is zero-padded to the length of the output signal, i.e. $L + M - 1$, followed by the application of the inverse Fourier transform and the multiplication with the frequency response of the filter before it is transformed back to the time domain. The final convolved signal will be the sum of the short convolutions [141], [145].

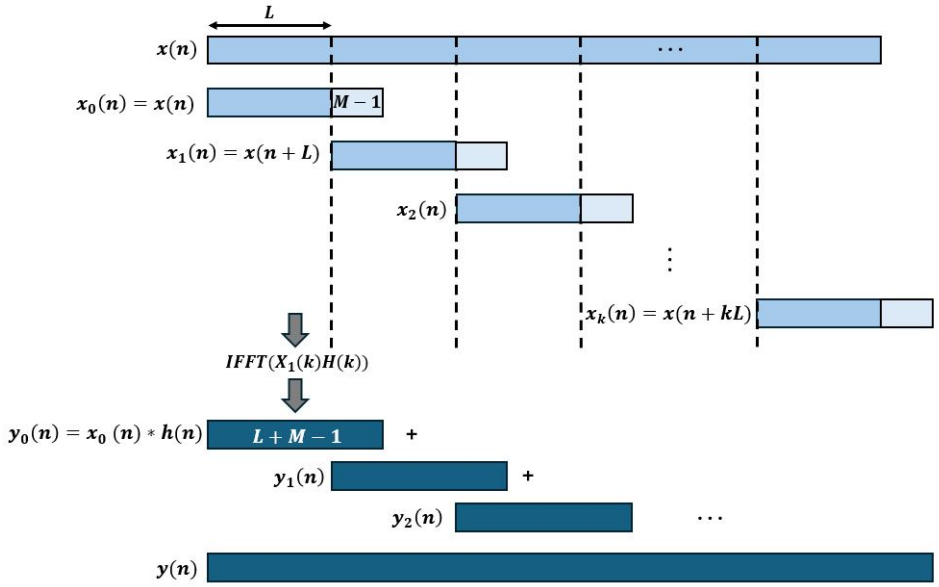

Figure 5.2: Overlap-add method. Figure adapted from [141].

5.3 Broadband noise synthesis

Broadband noise from CHOICE is estimated in 1/3 octave bands and can be synthesized using an overlap-add method [142], [146]. The process starts by summing the 1/3 octave band broadband noise spectra from all the components, at each time step. The total spectrum at each step is then converted to a narrowband spectrum with a frequency resolution that is dependent on the selected block size (or FFT length). The block size is selected to be larger than the time between two consecutive time steps which is called the hop size. The difference between the two determines the amount of overlap. It should be noted that the time step required for the auralization is much smaller than the one usually used for CHOICE, in order to eliminate audible artifacts when transitioning between time steps.

The narrowband spectrum at each time step is assigned a random phase and an inverse Fourier transform is applied to generate the time domain signal. The block signal is multiplied with a Hanning window and added to the previous block with a time delay that equals the hop size. In order to ensure correct acoustic energy values, the final signal is corrected for the amount of overlaps, as well as the window energy.

5.4 Tonal noise synthesis

Tonal noise for every component is synthesised using an additive synthesis technique [142], [146]. The pressure time history of each tone is, first, modelled as a cosine wave and the total noise is determined by summing all components as

$$p(t) = \sum_{i=1}^{N} A_i(t) \cos(2\pi f_i(t)t + \phi_i) \tag{5.8}$$

where $A_i(t)$ is the amplitude and $f_i(t)$ is the frequency of the i^{th} tone, with an initial phase ϕ_i. If there is no other information, the initial phase is usually assumed to be random.

Because CHOICE predicts noise in 1/3 octave band frequencies, the Doppler-shifted blade-passing-frequency and its harmonics, for every component (fan, compressor, etc.), are used to determine the frequency and amplitude of the tones in the predicted spectra [147]. This is performed at every time step or aircraft state which corresponds to the beginning of a synthesis block. In the additive synthesis technique, the synthesis block is equal to the hop size and there is no overlap needed to ensure a smooth transition. Instead, the tonal amplitudes and frequencies are smoothly varied between consecutive aircraft states via interpolation. The phase at the beginning of a synthesis block is also matched to the one at the end of the previous block, in order to avoid discontinuities between consecutive blocks.

5.5 Propagation effects

Propagation of the sound can be performed either prior to the synthesis operation or afterwards [142]. Both approaches should, theoretically, result in the same pressure

time history at the receiver. However, there are some benefits in using the time domain approach, i.e. applying the propagation subsequent to the synthesis. The main advantage is that it allows for imparting temporal variations, e.g. due to turbulence, and that it affects naturally any source noise unsteadiness [142]. Furthermore, the frequency domain propagation is usually performed in 1/3 octave band frequencies and is absent of phase. This has a negative effect on the frequency characteristics of the sound, as it disrupts the phase relationship between direct and ground reflected rays, leading to a more artificial sound.

In this work, two scenarios were tested. The first was the frequency domain approach as the propagation effects that were described in Section 4 are already included in the noise prediction in CHOICE, which outputs the receiver spectra at regular time intervals. The second scenario was a combination of the two approaches. The spreading loss and Doppler shift were applied in the frequency domain, as described in Section 4, while the atmospheric absorption and ground reflection, were applied in the time domain through filtering operations. The second approach was found to result in more realistic sounds. Therefore, any presented cases have been performed following this approach.

5.5.1 Atmospheric absorption filter

Atmospheric absorption is modelled according to the method presented in Section 4.2.2 and realized through an FIR filter, as described by Rietdijk [148] and Heutschi et al. [149]. The absorption spectrum is, firstly, determined as

$$H_{aa}(f) = 10^{-a(f)R/20} + 0j \tag{5.9}$$

where $a(f)$ is the absorption coefficient described by eq. 5.9 and R is the source receiver distance.

An Inverse Fourier transform was, then, applied to the spectrum to obtain the impulse response, which was circularly shifted in the time domain to obtain a causal filter with constant group delay. FFT convolution and the overlap-add method were used to apply the filter on the signal. To account for the delay caused by the filter, the first $M/2$ samples were dropped, where M is the length of the filter [148], [150].

5.5.2 Ground reflection filter

The ground reflection was considered through a reflection factor and a time delay applied on the direct path to obtain the reflected path. The fact that the same path was used for the direct and reflected wave is a fair approximation as the receiver height (typically between 1 and 2 m in this work) is much smaller than the source altitude. Hence, the difference in the directivity of the source will be small and can be ignored without impacting the result in a realizable manner.

As before, an FIR filter was created from the reflection coefficient described in eq. 4.5 of Section 4.2.3, by applying the inverse Fourier transform and shifting the impulse response by $M/2$ samples [150]. The reflected wave was calculated by convolving the filter with the direct path and dropping the first $M/2$ samples. This

was then added to the direct unfiltered wave with a delay of $round(F_s \Delta r/c)$ samples to obtain the final signal. Here, F_s is the sampling frequency, Δr the path-length difference, shown in Figure 4.2, and c the speed of sound.

In order to create a more realistic sound, turbulence was included in the ground reflection simulation. This was modelled according to the method proposed by Arntzen [146] where a turbulence-induced coherence loss factor was included in the ground reflection coefficient. Due to the fact that there were no available data on wind and temperature fluctuations, a weak turbulence was assumed. This factor only altered the ground interference pattern, making it less pronounced and improving the agreement with the measurements. However, for amplitude modulations due to atmospheric turbulence and wind, further assumptions and filters would need to be implemented which is not performed as part of the present work.

5.6 Comparative assessment of approach flyovers

In this section, a comparative assessment of synthesized spectrograms with recordings from flyover aircraft is performed. Three cases are presented corresponding to three of the flyovers that were performed as part of the ANT (Approach Noise Trials) project [151] at the CSA. The flights were performed using two Novair A321neo with LEAP-1A engines and all the measurements were taken during the morning of April 8th, 2021, at Arlanda airport, in Stockholm. These flights were conducted purely for noise measurement purposes and each aircraft performed 10 approach flyovers. 31 microphones were placed along a 15 nm approach path, mainly aligned with runway 26. The sampling frequency was 48 kHz with a frequency update of 125 ms. A detailed description of the measurement set up is presented by Åbom et al. [151], while details can also be found in Paper 4. FDR and noise measurement data for all flyovers and a number of recordings from selected microphone locations were available.

Figures 5.3-5.5 show the spectrograms for three synthesized and recorded approach flyovers. Figure 5.3 and Figure 5.4 correspond to a microphone located 4.7 nm from the runway threshold, at which point configuration 2 is selected and the landing gear is either extended before or during the pass-by of the aircraft above the microphone, while Figure 5.5 corresponds to a microphone 8 nm from the threshold, where configuration 2 is set. Although, the shapes of the synthesized spectrograms indicate a good agreement with the recorded ones, some notable differences can be noticed, for all three cases. The signal power in the low frequency region is somewhat overpredicted, especially in the first two cases, which could be attributed to the low frequency contribution from the landing gear component, as was shown in Paper 3. Furthermore, in the recorded spectrograms, some vertical lines can be observed which correspond to temporal variations at the source and temperature and wind fluctuations that affect the propagation [53], [146]–[148]. These are not present in the synthesized cases which are based on time-averaged models that do not include short term variations or atmospheric turbulence effects. The jumps that can be seen in the synthesized cases correspond to changes in the aircraft state, such as

change in configuration in Figure 5.3a and sudden increase or decrease in thrust in Figure 5.4a and Figure 5.5a. Another noticeable difference in all three cases is caused by the background noise in the recording (songbird, vegetation motion from the wind, etc.) which is seen as a higher frequency noise before and after the peak of the flyover aircraft noise. Finally, a difference in tonal components can be observed. In all three cases, some variable tones can be seen in the synthesis, which are related to harmonics of the BPF. These tones are slightly overpredicted, something that could be attributed to the simple noise suppression model and the fan prediction model which was developed based on an older engine. On the contrary, in the spectrograms of the recordings, some constant frequency tones can be noticed, that is if the frequency shift caused by the Doppler effect is overlooked. More specifically, in Figure 5.3b a constant frequency tone is observed at a frequency around 650 Hz at the beginning of the recording and in Figure 5.5b two constant frequency tones are seen at 350 Hz and 650 Hz. These are possibly attributed to cavities on the airframe such as the fuel vent opening on the wing [55], [56]. Another constant frequency tone can be noticed towards the end of the recording in Figure 5.3b, at a frequency around 1600 Hz. This seems to be close to the harmonic of the BPF but does not indicate any variation as is seen in Figure 5.3a. It is, therefore, likely to be caused by a cavity in the nose landing gear [54], [56].

The A-weighted sound pressure level as predicted by the synthesis for each of the three presented cases are compared with the measurements in Figure 5.6, and in Table 5.1, in terms of A-weighted sound exposure level and maximum noise level. It can be noticed that the agreement is good when the aircraft is close to the microphone while the two lines start to deviate when the aircraft is further away. From Figure 5.6a, Figure 5.6b and Table 5.1, it can be observed that the synthesized noise reaches slightly higher levels than the measured around the overhead point, while from Figure 5.6c it can be noticed that the forward radiated noise is somewhat overpredicted. As the aircraft moves away from the microphone, the synthesized noise level drops below the measured, for all three cases. This could partly be attributed to the presence of background noise in the measurements. Overall, these findings are in line with a previously published validation study of ANOPP [152]. It should be noted that since A-weighting has been used to compute the SPL, the low-frequency overprediction is somewhat suppressed in this comparison (the A-weighting curve reaches very low negative values in the low frequency region, as the human ear is less sensitive in this frequency region).

This comparison is a necessary first step towards the validation of the auralization model. However, further validation would require a subjective assessment via listening tests in order to determine the degree of realism of the synthesized sounds and to identify significant differences in the perception of the two sounds. Unfortunately, this could not be performed in the frame of the present project, as it was not originally planned. With regard to the comparisons, although there are some differences, mainly due to the limitations of the semi-empirical models, it is believed that the tool can be used for the relative assessment of different scenarios. Further improvement can also be achieved by implementing methods for propagation in non-standard atmosphere.

Table 5.1: A-weighted SEL and L_{Amax} for the synthesized and recorded flyover.

	SEL $[dB(A)]$		L_{Amax} $[dB(A)]$	
Case	Synth.	Meas.	Synth.	Meas.
1	81.16	79.20	71.99	70.45
2	81.81	79.92	72.63	71.93
3	72.54	72.80	61.14	64.43

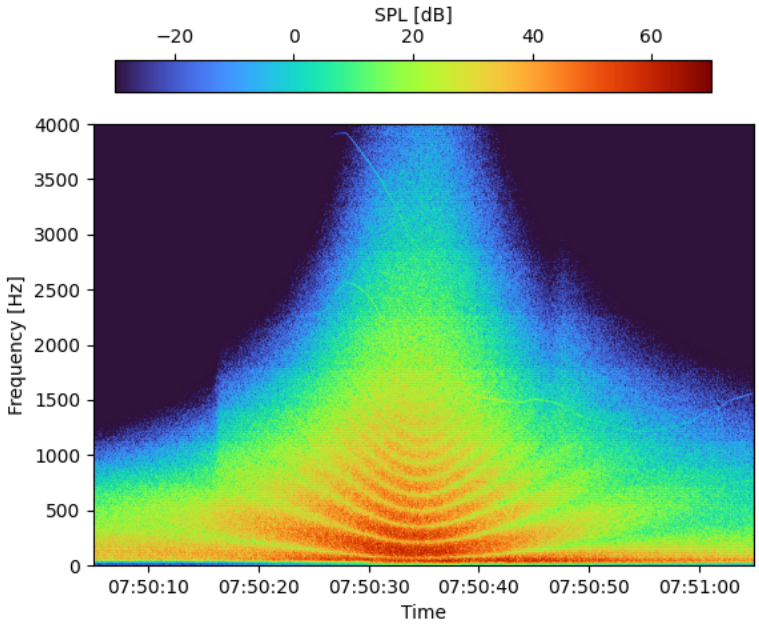

(a) Synthesized

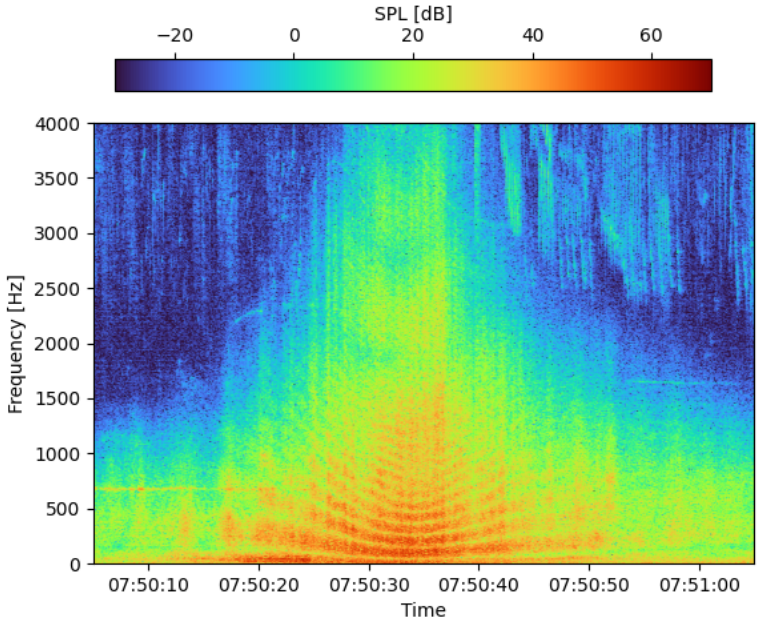

(b) Measured

Figure 5.3: Spectrograms of synthesized (a) and measured (b) aircraft flyover noise for case 1.

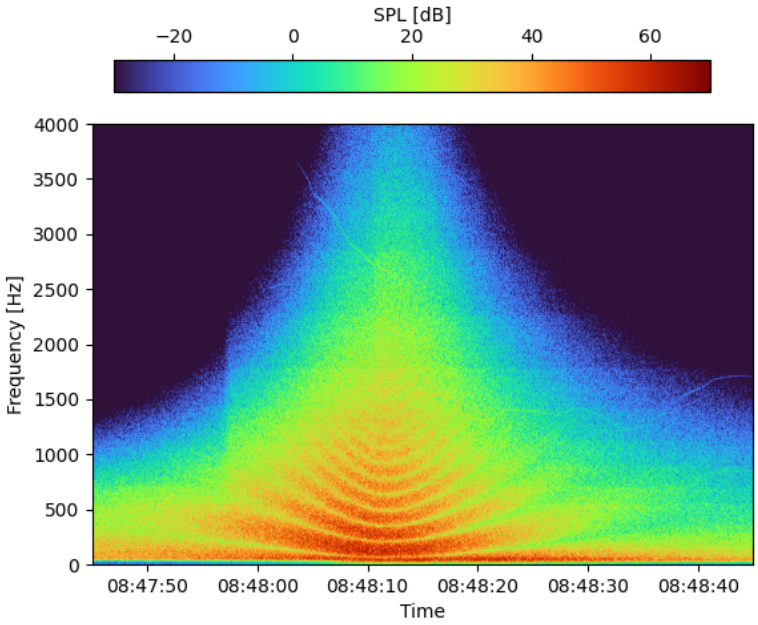

(a) Synthesized

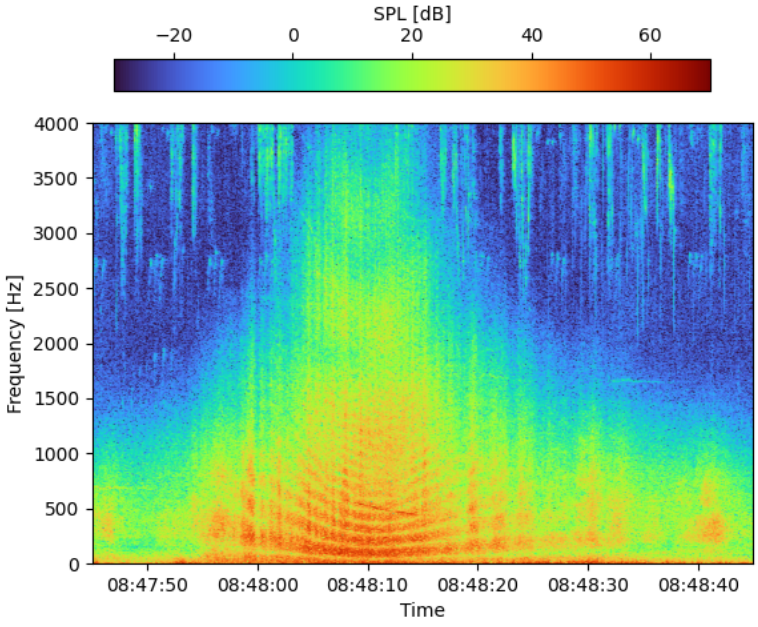

(b) Measured

Figure 5.4: Spectrograms of synthesized (a) and measured (b) aircraft flyover noise for case 2.

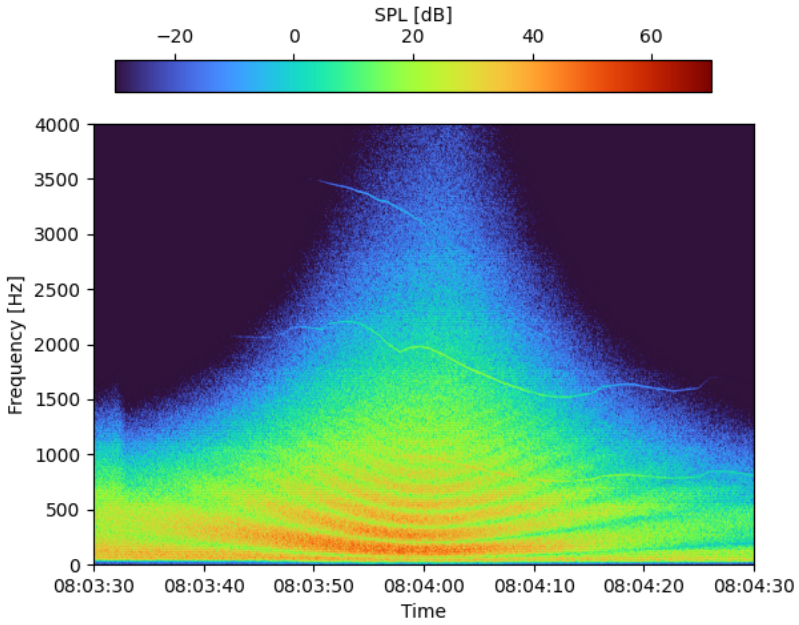

(a) Synthesized

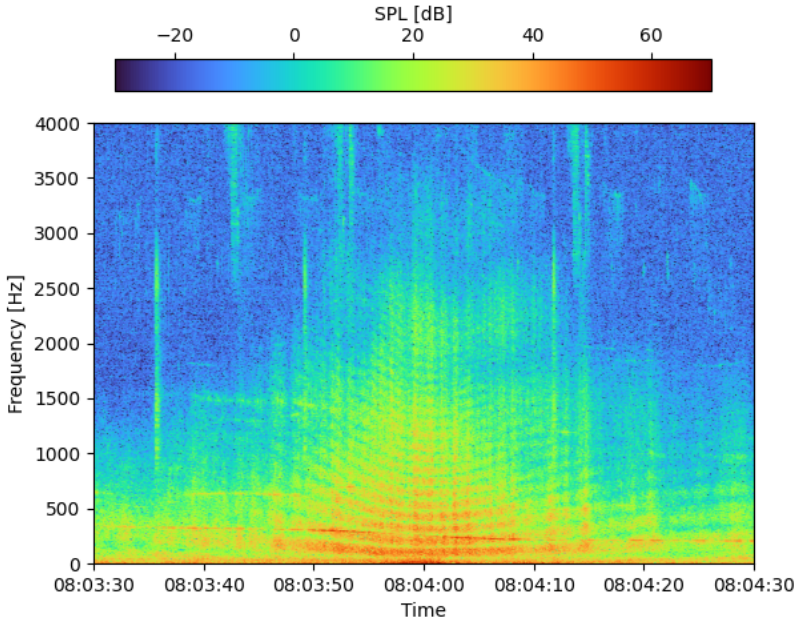

(b) Measured

Figure 5.5: Spectrograms of synthesized (a) and measured (b) aircraft flyover noise for case 3.

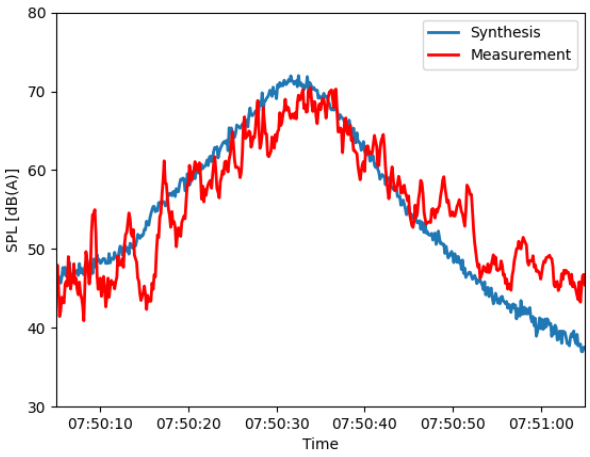

(a) Case 1

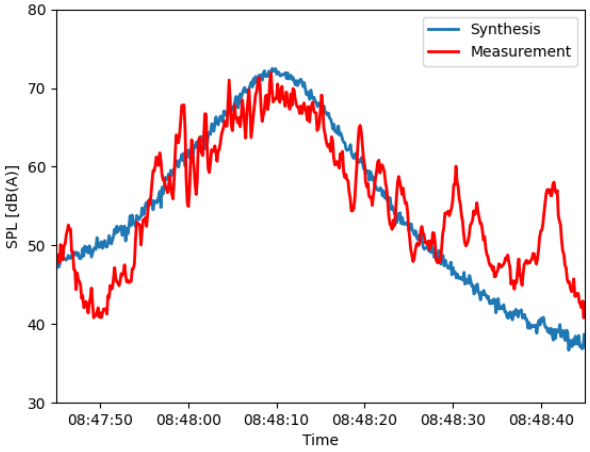

(b) Case 2

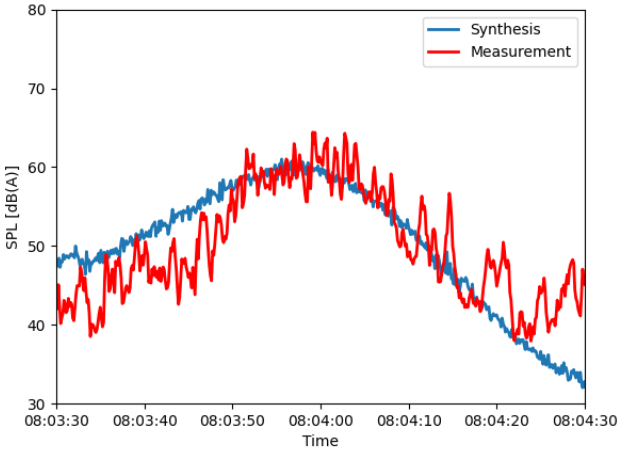

(c) Case 3

Figure 5.6: A-weighted sound pressure level for the synthesized and measured flyover noise.

Chapter 6
Summary of Papers

6.1 Paper 1

Thoma, E. M., Grönstedt, T., and Zhao, X., "Quantifying the Environmental Design Trades for a State-of-the-Art Turbofan Engine," *Aerospace*, Vol. 7, No. 10, 2020.

6.1.1 Division of work

All authors contributed to the development of the methodology and preparation of the manuscript. The author of the thesis performed the simulations, post-processed the results and wrote the original draft of the paper. Tomas Grönstedt contributed to the conceptualization and provided feedback on the manuscript. Xin Zhao contributed to the conceptualization, set up the optimization framework, validated the aircraft model, and provided feedback on the manuscript.

6.1.2 Aim

In Paper 1, a system-level study was performed in order to assess the environmental impact of early design choices for an ultra-high bypass ratio turbofan engine. The aim was to quantify the effect of engine cycle parameter variation on noise and NO_x emissions within a range close to the optimal engine condition where only a small penalty in fuel burn would be incurred.

6.1.3 Methodology description

For this study, a model was set up for a state-of-the-art single aisle thrust class turbofan engine. Component efficiencies, cooling technology, component weight and architecture were based on the Leap-1A engine. The aircraft system was modelled to match A321-200.

A Python-based framework combining several in-house codes was used to perform the simulations. The engine performance and design were evaluated using GESTPAN and WEICO. GESTPAN was also used to simulate the aircraft performance and establish trajectories by integrating the two dimensional flight dynamics equations. The computed trajectories concerned the LTO cycle and followed the noise

certification procedure guidelines. The engine cycle was optimized for minimum installed SFC (Specific Fuel Consumption), by allowing variation in OPR, FPR and BPR, while keeping the aircraft characteristics and the trajectories fixed. For the optimization, OpenMDAO was used, which is an open-source framework for multidisciplinary optimization, introduced by Gray et al. [153]. Around the optimum point, two case studies were defined, one for varying OPR and one for varying FPR and BPR. Trades were, then, evaluated between noise at the certification points and LTO emissions. Noise predictions were carried out using CHOICE and the methods presented in Chapter 3 and Chapter 4. NO_x emissions were computed using CHEESE (CHalmers Engine Emissions Simulation Environment) which is based on semi-empirical modeling methods [154].

6.1.4 Discussion

For the optimization, an installed SFC metric was selected as the objective function. This was expected to be a better metric than pure SFC as it accounts for the effect of the nacelle drag and engine weight. For both scenario studies, it was observed that with only a modest increase in the installed SFC metric, a large variation in cycle parameters could be achieved. This variation in engine parameters proved to be significant regarding the noise and emissions. Even though the OPR variation did not have a notable effect on noise, the decrease in total NO_x mass was significant, amounting to 12% reduction from the optimum installed SFC case. On the other hand, varying the fan diameter within a range not leading to a substantial increase in installed SFC resulted in an improvement in engine noise equal to 1.7 dB, and additionally giving a slight benefit in estimated NO_x emissions.

6.2 Paper 2

Thoma, E. M., Grönstedt, T., Otero, E., and Zhao, X., "Environmental Assessment of Noise Abatement Approach Trajectories," *33rd Congress of the International Council of the Aeronautical Sciences*, 2022.

6.2.1 Division of work

The author of the thesis formed and set up the scenario study, developed the trajectory model, the flight dynamics model and the optimization methodology, performed the simulations, post-processed the results and wrote the original draft of the paper. All co-authors provided support in the analysis and discussion and reviewed the manuscript.

6.2.2 Aim

In Paper 2, interdependencies between noise and emissions were evaluated for aircraft operational procedures. Focusing on approach procedures, the aim was to assess the

environmental impact of standard, more advanced and optimized noise abatement trajectories.

6.2.3 Methodology description

The trajectories were constructed based on available FDR data and theory found in operating manuals and similar studies. The ground path was kept constant for all study cases and only the vertical profile was varied according to the studied procedure. The aircraft performance was evaluated using the models developed in Chapter 2, followed by GESTPAN simulations to evaluate the engine performance and by CHOICE and CHEESE simulations for the prediction of noise and NO_x emissions. For this study, the noise mapping tool SAFT [155] was used in connection with CHOICE in order to generate SEL contours under the aircraft flight path.

An optimization study was performed using a multiobjective Genetic Algorithm. The objective was to minimize the noise impact for a community located underneath the flight path and the total mission NO_x emissions. The process started from a conventional approach trajectory and the objectives were normalized according to this procedure.

All cases were presented for an aircraft/engine model based on the A321neo with Leap-1A engine at Arlanda airport in Stockholm.

6.2.4 Discussion

Several approach procedures were evaluated for their environmental impact. The analysis started from noise abatement procedures, namely the CDA and LDLP, and other standard trajectories, such as the conventional and the multi-level approach. Based on these, more advanced trajectories were explored such as a CDA with a steeper descent angle, a segmented CDA and an LDLP with a shorter intermediate level segment. It was shown that there is no single better trajectory but the selection of the appropriate procedure is highly dependent on the airport, flight conditions, atmospheric conditions and aircraft type. From the results it was observed that, in general, if a procedure leads to noise reduction in proximity to the airport this is traded with increased noise level further away. The more advanced procedures seemed to result in increased NO_x emissions while the effect on the fuel consumption was not that evident. This can be explained by the fact that contrary to CO_2 and SO_x emissions, NO_x emissions also depend on the climate and local weather conditions.

As expected, the optimization resulted in the best solution from the studied trajectories and for the selected scenario. Even though noise was minimized for a specific location, an overall improvement was observed. NO_x emissions were significantly improved but a slight increase in the fuel consumption was observed, as it was not accounted for in the optimization. The increase in CO_2 and SO_x emissions was rather small and was considered acceptable for the achieved noise and NO_x emissions reduction.

6.3 Paper 3

Thoma, E. M., Grönstedt, T., Otero, E., and Zhao, X., "Assessment of an Open-Source Aircraft Noise Prediction Model Using Approach Phase Measurements," *Journal of Aircraft*, Articles in Advance, 2023.

6.3.1 Division of work

The author of the thesis contributed to the development of the code, established the validation process, performed the simulations, post-processed the results and wrote the original draft of the paper. Tomas Grönstedt contributed to the development of the original code, reviewed the manuscript and provided support in the analysis. Evelyn Otero provided support in the analysis and discussion and reviewed the work. Xin Zhao contributed to the development of the code, provided support in the analysis and feedback on the manuscript.

6.3.2 Aim

In Paper 3, a comparative assessment of an open-source aircraft noise prediction tool with flyover noise measurements for approach procedures was performed. The assessment was focused on the source noise level and was performed for every approach configuration separately, providing simulation details of noise generation of whole aircraft and key components breakdown. This way of validation provides an insight on the effect that variations in flight parameters and configuration settings have on noise.

6.3.3 Methodology description

The study was performed using flight data and ground-based noise measurements from 18 approach flights and 17 recording stations, positioned along the approach flight path. The flights were performed during one morning using two A321neo aircraft with Leap-1A engines at Arlanda Airport in Stockholm, with the purpose of collecting noise measurement data.

The source noise was calculated using the models that were described in Chapter 3. FDR data were used for the trajectory details and to predict the engine and aircraft performance parameters that are required for the noise prediction. The source noise prediction was then compared with the backpropagated noise measurements at the overhead point above each microphone. The assessment was performed for every high-lift device and landing gear setting, separately. For completeness, an assessment of the predicted ground noise level over time was also included. Finally, a sensitivity analysis was performed to study the effect of flight parameters variations on the source noise prediction.

6.3.4 Discussion

The predicted and measured sound spectra indicated an overall good agreement for the various configurations, especially in the mid-frequency region. Some deviations occurred in the low-frequency region, which is generally considered a region of high uncertainty. Configurations with a greater number of high-lift devices compared better with the measurements while the early configurations showed greater deviations. This was partly attributed to uncertainties caused by the increased aircraft-microphone distance for the latter. In general, it was shown that the source noise level can be predicted within 3 dB from the measurements, for most cases. The dependence on speed was found to be stronger for the source noise models which could be explained by the lack of installation effects in the modelling. Deviations could also occur due to the fact that the development of the models was based on older aircraft and engines, which lack noise suppression technologies. Despite the above limitations, the study showed that the models can be used to evaluate the noise form current aircraft with good accuracy.

6.4 Paper 4

Thoma, E. M., Johansson, A., Lin, X., Otero, E., "Flight Configuration-Based Analysis of Emissions and Noise Interdependencies" Manuscript under review in *Journal of Aircraft*, 2023.

6.4.1 Division of work

All authors contributed to the conceptualization, the development of the methodology and the analysis. The author of the thesis set up the code for the interdependencies' analysis, performed the simulations, post-processed the results and wrote the original draft of the paper. Anders Johansson performed the noise measurements and provided the post-processed data and contributed to writing of the original draft of the paper. Xiaoyi Lin set up the emissions simulations and performed an initial analysis on the emissions predictions. Evelyn Otero developed the emissions predictions model, coordinated the work and reviewed the manuscript.

6.4.2 Aim

In Paper 4, noise measurements and FDR data were used to examine the impact of variations in flight parameters on both noise level and emissions. The analysis was performed separately for every approach configuration, aiming to develop a better understanding of the complex interdependencies that arise between noise, CO_2 and non-CO_2 emissions.

6.4.3 Methodology description

The data used in this study are part of a noise measurement campaign (also used in Paper 3) that was developed during the pandemic with the aim to cover variations in speed, landing gear deployment, and approach altitude that are usually observed during normal approach procedures. FDR data from 18 test flights and noise measurements from all 31 recording stations were available for the analysis. The emissions were assessed based on fuel flow data derived from the FDR records and an emission prediction model, the Boeing Fuel Flow Method 2.

In the performed flight schedule, two altitude and four speed profiles are observed. The analysis was, thus, performed by separating the data into configurations, omitting transitional states, and, then, grouping the data according to their profiles. The noise was assessed based on the maximum A-weighted noise level on the ground and CO_2, H_2O, SO_x, CO, HC and NO_x emissions were calculated in terms of total produced amount, in kg, for each configuration segment.

6.4.4 Discussion

It was demonstrated that in early configurations, prior to landing gear deployment, there is a significant trade-off between CO_2, H_2O, SO_x and NO_x on one side and CO and HC on the other side, as the latter increase exponentially when low fuel flow levels are reached. On the contrary, ground noise level at this phase is primarily influenced by the aircraft-microphone distance and the atmospheric propagation effects. Therefore, minimum environmental impact can be reached by starting the approach from a higher altitude, followed by an idle power descent with careful consideration of the latter to prevent entering areas of critically low fuel flow. This can be avoided by, setting a minimum thrust threshold depending on the approach phase and flight configuration.

For the configurations that follow, the trade-off mainly lies between CO_2, H_2O, SO_x and NO_x emissions and noise as the drag increases causing an increase both in fuel consumption and noise level. With the extension of the landing gear, a significant dependency of the noise level on the aircraft speed is observed, amounting to an average increase of 1 dB for a 10 kn increase in speed. Hence, an obvious mitigation measure in this case is to reduce the flight speed, with a slight penalty in CO and HC emissions.

Overall, the study revealed that efforts aimed at reducing fuel consumption typically result in increased levels of CO and HC emissions, while trade-offs with regard to noise were more complex and highly dependent on the aircraft configuration.

6.5 Paper 5

Thoma, E. M., Merino-Martínez, R., Grönstedt, T., Zhao, X., “Noise from Flight Procedure Designed with Statistical Wind: Auralization and Psychoacoustic Evaluation” Accepted and to be presented on the *30th AIAA/CEAS Aeroacoustics Conference* and subsequently to be submitted to an AIAA journal for consideration, 2024.

6.5.1 Division of work

The author of the thesis contributed to the conceptualization, developed the noise prediction and auralization code, performed the simulations, post-processed the results and wrote the original draft of the paper. Roberto Merino-Martinez supervised the work on the development of the auralization code, provided the prediction method and results for the sound quality metrics, wrote part of the paper and provided feedback. Tomas Grönstedt supported the analysis and reviewed the paper. Xin Zhao contributed to the conceptualization, provided the study case, contributed to the development of the framework, supported the discussion and provided feedback.

6.5.2 Aim

In Paper 5, two approach procedures that were designed following different design methodologies were assessed for their noise impact on the near-airport communities. The assessment included an analytic comparison with both conventional and sound quality metrics. The aim was to evaluate the potential noise benefits of the new design, not only through quantitative metrics but also through the evaluation of the perceived annoyance.

6.5.3 Methodology description

The study focused on two Required Navigation Performance Authorization Required (RNP AR) approach procedures designed following the ICAO regulations. According to these regulations, the design can be based on standardized meteorological conditions or historical data specific to the procedure location, with the former being the more common approach. The two designs inevitably resulted in different lateral profiles which were expected to lead to variations in community noise impact.

These differences were evaluated using the methods outlined in this thesis. Initially, a quantitative analysis was conducted by generating sound exposure contours and estimating the difference in the amount of highly affected population. This was followed by a perception-based evaluation for the residents of selected locations, utilizing auralization and psychoacoustic assessment to determine the level of annoyance experienced by individuals in these areas. The psychoacoustic assessment was performed with the help of sound quality metrics that were calculated using the open-source MATLAB toolbox SQAT (Sound Quality Analysis Toolbox) v1.0 [156].

6.5.4 Discussion

It was demonstrated that with the reconstruction of the lateral profile of the procedure a notable decrease in the number of noise-affected people could be achieved, amounting to about 1/3 of the initially affected population. However, this adjustment, caused by the reduction in aircraft turn radius, resulted in the displacement of the noise contour towards urban areas that were previously less-severely affected. This gave rise to the question of whether it is ethical to change the existing procedure. The perception-based analysis was performed with the aim of providing more details and

facilitating the decision-making process involving this question. The auralizations and the calculation of the psychoacoustic metrics were performed at three selected points and revealed minor differences in audible noise levels and annoyance, with the new procedure suggesting slightly lower levels at the most severely affected locations. Although, this came at the expense of a notable increase in annoyance for the residents of the previously less-severely affected area.

Chapter 7
Concluding Remarks

7.1 Summary

The present work has focused on different aspects involved in aircraft noise mitigation. These included the development of a comprehensive aircraft noise prediction tool, the investigation of noise mitigation strategies through experimental data and available models, and the evaluation of noise reduction scenarios at the source or through flight path management.

The source noise prediction was described in Chapter 3 and was based on empirical and semi-empirical models, which can be found in the public literature. These models require detailed input with regard to the engine and aircraft performance which was provided from the developed trajectory model and the in-house performance tools that were presented in Chapter 2. This consisted the first part of the aircraft noise prediction tool-chain which, despite the limitations of the models (discussed in Section 3.2.3), was shown, from the study in Paper 3, to provide a good estimation of the noise generated from current aircraft and to capture the effect of variations in flight parameters and configuration well. For the propagation of the sound a standard atmosphere with no wind was assumed and accounting for the effects described in Chapter 4 the noise on the ground was predicted, either at a selected microphone location or by generating noise exposure contours. The propagation method was assessed as part of Paper 1 and Paper 3 and showed a good agreement with certification data and measurements, respectively.

Using the described methods, two scenario studies were performed. The first study, presented in Paper 1, was focused on noise reduction at the source and, more specifically, how it can be achieved at an early design stage of current state-of-the-art engines for a minimum impact in fuel burn. It was demonstrated that for only a modest effect on the fuel burn, a relatively large variation in engine cycle parameters is allowed, which can result in reduction in noise, as well as, NO_x emissions.

The second scenario study, included in Paper 2, was focused on the operational aspect and on the environmental impact of modifications in approach trajectories and procedures, involving the evaluation of interdependencies between noise, CO_2, and non-CO_2 emission. Through the various procedure designs and the multidisciplinary

optimization, it was shown that, if the design is adapted to specific airport and conditions, significant improvement can be achieved in both noise and emissions.

The operational aspect was further investigated, somewhat indirectly in Paper 3, and with the help of experimental data, in Paper 4. In the former, through the configuration-based validation and the source noise breakdown, it was possible to evaluate not only the impact of each configuration change on noise level, but also how variations in flight parameters, such as speed and thrust, affect noise within the same configuration. The assessment was performed both with experimental data and with predictions from the semi-empirical models, and clearly demonstrated the increasing impact of speed as higher configurations are used, while the effect of thrust was only found relevant for the Clean configuration. Similar findings were observed in Paper 4. In particular, using noise measurement data from a flight schedule that was developed to cover variations in speed, altitude and landing gear deployment position within the range typically found in a normal approach, it was possible to closely study the trade-offs between noise and emissions. This assessment showed that in early configurations prior to landing gear deployment, there's a significant trade-off between CO_2, H_2O, SO_x, and NO_x emissions versus CO and HC emissions, while ground noise levels are primarily influenced by aircraft-microphone distance and atmospheric propagation effects. In subsequent configurations, the trade-off shifts to primarily between CO_2, H_2O, SO_x, and NO_x emissions and noise, with increased drag leading to higher fuel consumption and noise levels.

For all previous studies, conventional metrics were used for the assessment, which, although, very important and necessary, do not provide much information on the human perception of the noise. Thus, the noise prediction was further improved through the integration of auralization, which was described in Chapter 5. When auralizations of real flyovers were compared with the corresponding recordings, a few audible differences could be noted, despite that the noise metrics for each flyover were generally well predicted. The most distinct differences, apart from the lack of background noise in the synthesis, was the absence of amplitude modulations caused by temporal variations at the source and turbulence effects in the propagation, as well as differences in the tonal components. Including more complex propagation effects, such as wind and turbulence, could potentially improve the agreement between the auralizations and the recordings, although, the former will always be limited by the assumptions and the level of detail included in the semi-empirical source noise prediction. As the noise prediction is performed in 1/3 octave band frequencies, some frequency information is inevitably lost, thus, affecting the auralization that requires narrowband information. Despite the noted differences and limitations, it is believed that the tool can be used for the relative assessment of different scenarios.

Using the whole tool-chain, another scenario study with a focus on the operational aspect was performed in Paper 5. The assessment involved two RNP AR approach procedures that were designed following the ICAO regulations for procedure design. These were compared in terms of sound exposure level, amount of affected population, auralizations and perceived-annoyance. It was shown that this kind of assessment could provide valuable input during the procedure design and facilitate the decision-making process for standardizing a procedure.

7.2 Future work

During this work, some challenges and opportunities for further research were identified. These include both modelling and prediction related challenges and opportunities for noise mitigation related research. Based on these, some recommendations are made which are separated according to the relevant topic and presented below.

Source noise prediction: Performing a similar validation study for conditions where the engine noise is dominant, e.g. during take-off, could contribute in identifying limitations and further improving the implemented engine models. This improvement, could be achieved by developing more analytical models for the acoustic treatment mechanisms and including a more detailed description of installation and interaction effects. For this purpose, experimental data from departure procedures or from test facilities would facilitate the work.

Noise propagation: For real life applications, it would be useful to further develop the noise propagation methodology to account for a non-standard atmosphere by including the effect of wind and changes in atmospheric temperature and pressure, while the accuracy of the noise contours could be further improved by incorporating terrain information.

Auralization: The recommendations for advancing the noise propagation would also contribute in more realistic synthesized sounds, which could be further improved by including temporal variations at the source. In addition, a very useful assessment and a next step would be to conduct listening experiments in order to evaluate the degree of realism of the auralizations and to develop an understanding of the human response to different sounds.

Scenario studies: Although the implemented semi-empirical models have limited capabilities in assessing advanced future aircraft concepts, with some modifications they are able to predict the noise from other future technologies, such as boundary layer ingestion (BLI) propulsion and propeller driven electric aircraft. Electric aircraft, especially, have gained a lot of interest in Sweden, and an assessment of their noise impact could be performed, ideally in collaboration with external partners.

Bibliography

[1] "Burden of disease from environmental noise - Quantification of healthy life years lost in Europe," WHO Regional Office for Europe, Tech. Rep., 2011, ISBN: 9789289002295. [Online]. Available: https://www.who.int/publications-detail-redirect/9789289002295 (visited on 02/03/2024).

[2] World Health Organization Europe (WHO), "Environmental Noise Guidelines for the European Region," WHO Regional Office for Europe, Copenhagen, Denmark, Tech. Rep. ISBN 978 92 890 5356 3, 2018.

[3] M. Basner, C. Clark, A. Hansell, J. I. Hileman, S. Janssen, K. Shepherd, and V. Sparrow, "Aviation Noise Impacts: State of the Science," *Noise & Health*, vol. 19, no. 87, pp. 41–50, 2017, ISSN: 1463-1741. DOI: 10.4103/nah.NAH_104_16.

[4] T. Elliff, M. Cremaschi, and V. Huck, "Impact of aircraft noise pollution on residents of large cities," Policy Department for Citizens' Rights and Constitutional Affairs, European Parliament, Brussels, Tech. Rep. PE 650.787, Jan. 2021. [Online]. Available: https://www.europarl.europa.eu/RegData/etudes/STUD/2020/650787/IPOL_STU(2020)650787_EN.pdf.

[5] EASA, "European Aviation Environmental Report 2022," European Union Aviaion Safety Agency (EASA), Tech. Rep. 978-92-9210-225-8, 2022.

[6] *Health impacts of exposure to noise from transport*, en, Jul. 2022. [Online]. Available: https://www.eea.europa.eu/en/analysis/indicators/health-impacts-of-exposure-to-1 (visited on 02/04/2024).

[7] *Noise data reported under Environmental Noise Directive (END)*, Dec. 2021. [Online]. Available: https://www.eea.europa.eu/en/datahub/datahubitem-view/c952f520-8d71-42c9-b74c-b7eb002f939b?activeAccordion=1084441%2C1070003 (visited on 02/04/2024).

[8] *Aircraft Noise*, Accessed in January 2024. [Online]. Available: https://www.icao.int/environmental-protection/pages/noise.aspx (visited on 04/27/2022).

[9] "Annex 16 - Environmental Protection - Volume I - Aircraft Noise," International Civil Aviation Organization (ICAO), Montréal, Quebec, Canada, Tech. Rep. ISBN 978-92-9258-260-9, Jul. 2017.

[10] "Doc 9501, Environmental Technical Manual - Volume I - Procedures for the Noise Certification of Aircraft," International Civil Aviation Organization (ICAO), Montréal, Quebec, Canada, Tech. Rep., 2018.

[11] A. Filippone, "Aircraft noise prediction," *Progress in Aerospace Sciences*, vol. 68, pp. 27–63, Mar. 2014. DOI: 10.1016/j.paerosci.2014.02.001.

[12] "Airports Commission: Final report," Airports Commission, London, UK, Tech. Rep. ISBN: 978-1-84864-158-7, Jul. 2015.

[13] J. I. Hileman, Z. S. Spakovszky, M. Drela, M. A. Sargeant, and A. Jones, "Airframe Design for Silent Fuel-Efficient Aircraft," *Journal of Aircraft*, vol. 47, no. 3, pp. 956–969, 2010, ISSN: 0021-8669. DOI: 10.2514/1.46545.

[14] S. Mistry, H. Smith, and J. P. Fielding, "Novel Design Concepts for Aircraft with Reduced noise and Global Warming Characteristics," in *26th Congress of the International Council of the Aeronautical Sciences ICAS 2008*, Anchorage, Alaska, USA, Sep. 2008, ISBN: 0-9533991-9-2.

[15] N. Cumpsty, D. Mavris, and M. Kirby, "Aviation and the Environment: Outlook," ICAO, Environmental Report, 2019, pp. 24–38. [Online]. Available: https://www.icao.int/environmental-protection/Documents/EnvironmentalReports/2019/ENVReport2019_pg24-38.pdf.

[16] P. R. Gliebe and B. A. Janardan, "Ultra-High Bypass Engine Aeroacoustic Study," General Electric Aircraft Engines, Cincinnati, OH, United States, Technical Report NASA/CR-2003-212525, E-14087, Oct. 2003.

[17] X. Liu, D. Zhao, D. Guan, S. Becker, D. Sun, and X. Sun, "Development and progress in aeroacoustic noise reduction on turbofan aeroengines," *Progress in Aerospace Sciences*, vol. 130, Apr. 2022. DOI: 10.1016/j.paerosci.2021.100796.

[18] *The 'Silent' Aircraft Initiative*, 2006. [Online]. Available: http://silentaircraft.org/.

[19] "Doc 9184, Airport Planning Manual - Part II - Land Use and Environmental Management," International Civil Aviation Organization (ICAO), Montréal, Quebec, Canada, Manual ISBN 978-92-9258-645-4, 2018.

[20] H. Yu, E.-J. Van Kampen, and J. A. Mulder, "An Optimization Paradigm for Arrival Trajectories using Trajectory Segmentation and State Parameterization," San Diego, California, USA, Jan. 2016. DOI: https://doi.org/10.2514/6.2016-1872.

[21] M. Zhang and A. Filippone, "Optimum problems in environmental emissions of aircraft arrivals," *Aerospace Science and Technology*, vol. 123, Apr. 2022. DOI: 10.1016/j.ast.2022.107502.

[22] H. G. Visser and R. A. A. Wijnen, "Optimization of Noise Abatement Departure Trajectories," *Journal of Aircraft*, vol. 38, no. 4, pp. 620–627, Jul. 2001. DOI: 10.2514/2.2838.

[23] M. Zhang, A. Filippone, and N. Bojdo, "Multi-objective optimisation of aircraft departure trajectories," *Aerospace Science and Technology*, vol. 79, pp. 37–47, Aug. 2018. DOI: 10.1016/j.ast.2018.05.032.

[24] D. S. Zachary, J. Gervais, and U. Leopold, "Multi-impact optimization to reduce aviation noise and emissions," *Transportation Research Part D: Transport and Environment*, vol. 15, no. 2, pp. 82–93, Mar. 2010. DOI: https://doi.org/10.1016/j.trd.2009.09.005.

[25] R. Koenig and O. Macke, "Evaluation of simulator and flight tested noise abatement approach procedures," in *ICAS 2008-4.8.1*, Anchorage, Alaska, USA, Sep. 2008.

[26] "Doc 8168, Procedures for Air Navigation Services - Aircraft Operations Volume I - Flight Procedures - Sixth Edition," International Civil Aviation Organization (ICAO), Montréal, Quebec, Canada, Tech. Rep. ISBN 978-92-9258-670-6, 2018.

[27] "Doc 9889, Airport Air Quality Manual - Second Edition," International Civil Aviation Organization (ICAO), Montréal, Quebec, Canada, Tech. Rep. ISBN 978-92-9258-963-9, 2020.

[28] "Doc 9613, Performance-based navigation (PBN) manual - Third Edition," International Civil Aviation Organization (ICAO), Montréal, Quebec, Canada, Tech. Rep. ISBN 978-92-9231-198-8, 2008.

[29] "Doc 9905, Required Navigation Performance Authorization Required (RNP AR) Procedure Design Manual - Third Edition," International Civil Aviation Organization (ICAO), Montréal, Quebec, Canada, Tech. Rep. ISBN 978-92-9265-613-3, 2021.

[30] "Doc 9931, Continuous Descent Operations (CDO) Manual," International Civil Aviation Organization (ICAO), Montréal, Quebec, Canada, Tech. Rep. ISBN 978-92-9231-640-2, 2010.

[31] "Doc 9993, Continuous Climb Operations (CCO) Manual," International Civil Aviation Organization (ICAO), Montréal, Quebec, Canada, Tech. Rep. ISBN 978-92-9249-255-7, 2013.

[32] *Area Navigation Systems | SKYbrary Aviation Safety*, Accessed in February 2024. [Online]. Available: https://skybrary.aero/articles/area-navigation-systems (visited on 02/10/2024).

[33] "Destination 2050 – A route to net zero European aviation," NLR – Royal Netherlands Aerospace Centre, SEO Amsterdam Economics, Tech. Rep. NLR-CR-2020-510, Feb. 2021.

[34] *2050 long-term strategy - European Commission*, Accessed in February 2024. [Online]. Available: https://climate.ec.europa.eu/eu-action/climate-strategies-targets/2050-long-term-strategy_en (visited on 02/12/2024).

[35] U. Nations, *The Paris Agreement*, en, Publisher: United Nations. [Online]. Available: https://www.un.org/en/climatechange/paris-agreement (visited on 02/12/2024).

[36] *ACARE Goals - Acare*. [Online]. Available: https://www.acare4europe.org/acare-goals/.

[37] A. Miele, *Flight Mechanics: Theory of Flight Paths* (Dover Books on Aeronautical Engineering). Mineola, New York: Dover Publications, Inc., Apr. 2016, ISBN: 9780486801469.

[38] W. S. Alexander and O. M. Klose, "The Relationship of Wind Correction Angle to Drift Angle," *Journal of the Aeronautical Sciences*, vol. 8, no. 11, pp. 409–412, Nov. 1940. DOI: 10.2514/8.10761.

[39] *ANP legacy data | EASA*, accessed in January 2024, Aug. 2023. [Online]. Available: https://www.easa.europa.eu/en/domains/environment/policy-support-and-research/aircraft-noise-and-performance-anp-data/anp-legacy-data#group-easa-dataset (visited on 01/02/2024).

[40] *A321neo | A320 | Aircraft | Airbus Aircraft*, Section: Aircraft, Oct. 2021. [Online]. Available: https://aircraft.airbus.com/en/aircraft/a320-the-most-successful-aircraft-family-ever/a321neo (visited on 01/08/2024).

[41] *Airbus A321neo*, accessed in January 2024, Dec. 2023. [Online]. Available: https://en.wikipedia.org/w/index.php?title=Airbus_A321neo&oldid=1192551864 (visited on 01/02/2024).

[42] "TCDS EASA.A.064 - Airbus A318, A319, A320, A321 Single Aisle," European Union Aviation Safety Agency, Blagnac, France, Type Certificate Data Sheet EASA.A.064, Feb. 2023. [Online]. Available: https://www.easa.europa.eu/en/document-library/type-certificates/noise/easaa064-airbus-a318-a319-a320-a321-single-aisle (visited on 12/07/2023).

[43] T. Grönstedt, "Development of methods for analysis and optimization of complex jet engine systems," ISBN 91-7197-910-7, Ph.D. Thesis, Chalmers University of Technology, Gothenburg, Sweden, 2000.

[44] T. Grönstedt, D. Au, K. G. Kyprianidis, and S. Ogaji, "Low-Pressure System Component Advancements and Its Influence on Future Turbofan Engine Emissions," in *Proceedings of ASME Turbo Expo 2009: Power for Land, Sea and Air*, Orlando, Florida, USA, Jun. 2009. DOI: 10.1115/GT2009-60201.

[45] *LEAP Overview CFM International*, 2017. [Online]. Available: https://www.cfmaeroengines.com/wp-content/uploads/2017/09/Brochure_LEAPfiches_2017.pdf.

[46] R. Stickles and J. Barrett, "TAPS II Technology Final Report – Technology Assessment Open Report," en, Federal Aviation Administration (FAA), Washington, DC 20591, Tech. Rep. DTFAWA-10-C-00046, Jun. 2013.

[47] *ICAO Aircraft Engine Emissions Databank | EASA*, accessed in January 2024, Jun. 2023. [Online]. Available: https://www.easa.europa.eu/en/domains/environment/icao-aircraft-engine-emissions-databank (visited on 01/02/2024).

[48] G. J. J. Ruijgrok, *Elements of Aviation Acoustics*. Delft, the Netherlands: Delft University Press, 1993, ISBN: 90-6275-899-1.

[49] L. Bertsch, M. Snellen, L. Enghardt, and C. Hillenherms, "Aircraft Noise Generation and Assessment: Executive Summary," *CEAS Aeronautical Journal*, vol. 10, pp. 3–9, Mar. 2019. DOI: 10.1007/s13272-019-00384-3.

[50] D. V. Zante, D. E. VanZante, D. Nark, and H. Fernandez, "Propulsion Noise Reduction Research in the NASA Advanced Air Transport Technology Project," GRC-E-DAA-TN43850, Manchester, UK: NASA, 2017.

[51] "Discussion Paper 05: Aviation noise," Airports Commission, London, UK, Tech. Rep., Jul. 2013. [Online]. Available: https://www.thenbs.com/publicationindex/documents/details?Pub=AIRC&DocId=304075 (visited on 01/30/2024).

[52] *Boeing 247 set the tone for airliners — General Aviation News*, en-US, Mar. 2020. [Online]. Available: https://generalaviationnews.com/2020/03/29/boeing-247-set-the-tone-for-airliners/ (visited on 01/08/2024).

[53] M. P. Allen, "Analysis and Synthesis of Aircraft Engine Fan Noise for Use in Psychoacoustic Studies," M.S. thesis, Virginia Polytechnic Institute and State University, Blacksburg, Virginia, Apr. 2012.

[54] R. Merino-Martinez and M. Snellen, "Implementation of tonal cavity noise estimations in landing gear noise prediction models," in *AIAA AVIATION 2020 FORUM*, ser. AIAA 2020-2578, American Institute of Aeronautics and Astronautics, Jun. 2020. DOI: 10.2514/6.2020-2578. (visited on 12/05/2023).

[55] R. Pieren, L. Bertsch, D. Lauper, and B. Schäffer, "Improving future low-noise aircraft technologies using experimental perception-based evaluation of synthetic flyovers," *Science of The Total Environment*, vol. 692, pp. 68–81, Nov. 2019, ISSN: 0048-9697. DOI: 10.1016/j.scitotenv.2019.07.253.

[56] W. Dobrzynski, "Almost 40 Years of Airframe Noise Research: What Did We Achieve?" *Journal of Aircraft*, vol. 47, no. 2, pp. 353–367, Mar. 2010, Publisher: American Institute of Aeronautics and Astronautics, ISSN: 0021-8669. DOI: 10.2514/1.44457.

[57] R. G. Rackl, G. Miller, Y. Guo, and K. Yamamoto, "Airframe Noise Studies: Review and Future Direction," NASA Langley Research Center, Hampton, Virginia, Contractor Report (CR) NASA/CR-2005-213767, Jun. 2005.

[58] L. Bertsch, D. G. Simons, and M. Snellen, "Aircraft Noise: The major sources, modelling capabilities, and reduction possibilities," German Aerospace Center & Delft Technical University, Göttingen, Germany, Monograph DLR IB 224-2015 A 110, 2015. DOI: 10.34912/ac-n0is3.

[59] F. Farassat and J. H. Casper, "Towards an airframe noise prediction methodology: Survey of current approaches," *Collection of Technical Papers - 44th AIAA Aerospace Sciences Meeting*, vol. 4, pp. 2496–2507, 2006. DOI: 10.2514/6.2006-210.

[60] L. Bertsch and U. Isermann, "Noise prediction toolbox used by the DLR aircraft noise working group," in *INTER-NOISE 2013, the 42nd International Congress and Exposition on Noise*, Reston, VA: Inst. of Noise Control Engineering, Sep. 2013, pp. 805–813.

[61] W. E. Zorumski, "Aircraft noise prediction program theoretical manual, Parts 1 and 2," NASA, Hampton, VA, United States, Technical Memorandum 83199, Feb. 1982.

[62] L. Bertsch, W. Dobrzynski, and S. Guérin, "Tool Development for Low-Noise Aircraft Design," *Journal of Aircraft*, vol. 47, no. 2, pp. 694–699, Mar. 2010. DOI: 10.2514/1.43188.

[63] W. L. Willshire Jr. and D. P. Garber, "Advanced Subsonic Transport Approach Noise: The Relative Contribution of Airframe Noise," NASA Langley Research Center, Hampton, VA, United States, Technical Memorandum NASA-TM-104112, Jun. 1992.

[64] R. H. Thomas, C. L. Burley, and C. L. Nickol, "Assessment of the Noise Reduction Potential of Advanced Subsonic Transport Concepts for NASA's Environmentally Responsible Aviation Project," in *54th AIAA Aerospace Sciences Meeting*, ser. AIAA SciTech Forum, San Diego, California: American Institute of Aeronautics and Astronautics, Jan. 2016. DOI: 10.2514/6.2016-0863.

[65] L. Bertsch, W. Heinze, and M. Lummer, "Application of an Aircraft Design-To-Noise Simulation Process," in *14th AIAA Aviation Technology, Integration, and Operations Conference*, ser. AIAA AVIATION Forum, American Institute of Aeronautics and Astronautics, Jun. 2014. DOI: 10.2514/6.2014-2169.

[66] M. Nöding and L. Bertsch, "Application of Noise Certification Regulations within Conceptual Aircraft Design," en, *Aerospace*, vol. 8, no. 8, p. 210, Aug. 2021, Number: 8 Publisher: Multidisciplinary Digital Publishing Institute, ISSN: 2226-4310. DOI: 10.3390/aerospace8080210.

[67] L. Lopes and C. Burley, "Design of the Next Generation Aircraft Noise Prediction Program: ANOPP2," in *17th AIAA/CEAS Aeroacoustics Conference*, Portland, Oregon: American Institute of Aeronautics and Astronautics, Jun. 2011. DOI: 10.2514/6.2011-2854.

[68] European Civil Aviation Conference (ECAC), "Report on Standard Method of Computing Noise Contours around Civil Airports, 4th Edition," European Civil Aviation Conference, Neuilly-sur-Seine Cédex, France, Tech. Rep., Dec. 2016. [Online]. Available: https://www.ecac-ceac.org/images/documents/ECAC-Doc_29_4th_edition_Dec_2016_Volume_3_Part_1.pdf.

[69] E. R. Boeker, E. Dinges, B. He, G. Fleming, C. Roof, P. Gerbi, A. S. Rapoza, and J. Hemann, "Integrated Noise Model (INM) Version 7.0 Technical Manual," Office of Environment and Energy, Federal Aviation Administration (FAA), Washington DC, USA, Tech. Rep., Jan. 2008.

[70] Federal Aviation Administration (FAA), *Aviation Environmental Design Tool (AEDT) Version 3d*. [Online]. Available: https://aedt.faa.gov/3d_information.aspx (visited on 04/27/2022).

[71] E. M. Thoma, X. Zhao, and T. Grönstedt, *CHOICE - CHalmers nOIse CodE*, Accessed in December 2023, Dec. 2022. [Online]. Available: https://github.com/emthm/CHOICE (visited on 12/06/2023).

[72] J. F. Groeneweg and E. J. Rice, "Aircraft Turbofan Noise," *Journal of Turbomachinery*, vol. 109, no. 1, pp. 130–141, Jan. 1987. DOI: 10.1115/1.3262058.

[73] M. F. Heidmann, "Interim Prediction Method for Fan and Compressor Source Noise," NASA, Lewis Research Center, Cleveland, Ohio, Technical Memorandum (TM) NASA-TM-X-71763, Jun. 1979.

[74] K. B. Kontos, B. A. Janardan, and P. R. Gliebe, "Improved NASA-ANOPP Noise Prediction Computer Code for Advanced Subsonic Propulsion Systems," NASA Lewis Research Center, Cincinnati, OH United States, Contractor Report 195480, Aug. 1996.

[75] A. P. Dowling and Y. Mahmoudi, "Combustion noise," *Proceedings of the Combustion Institute*, vol. 35, no. 1, pp. 65–100, Jan. 2015, ISSN: 1540-7489. DOI: 10.1016/j.proci.2014.08.016.

[76] A. H. Marsh and G. L. Blankenship, "Review of Turbofan-Engine Combustion and Jet-Noise Research and Related Topics.," DyTech Engineering, Inc., Long Beach, CA, Tech. Rep. FAA-RD80-16, Jan. 1980.

[77] P. Gliebe, R. Mani, H. Shin, B. Mitchell, G. Ashford, S. Salamah, and S. Connell, "Aeroacoustic Prediction Codes," NASA, Glenn Research Center, Contractor Report NASA/CR-2000-210244, 2000.

[78] P. Gliebe, R. Mani, S. Connell, S. Salamah, J. Sober, and R. Coffin, "AST Critical Propulsion and Noise Reduction Technologies for Future Commercial Subsonic Engines Aeroacoustic Prediction Codes - Supplement: Code Descriptions and Users Guides," NASA Glenn Research Center, Cleveland, Ohio, Contractor Report (CR) NASA-CR-20220004640, Tech. Rep., Apr. 2022.

[79] E. A. Krejsa and M. F. Valerino, "Interim prediction method for turbine noise," NASA Lewis Research Center, Cleveland, OH, United States, Technical Memorandum NASA-TM-X-73566, Nov. 1976.

[80] D. G. Dunn and N. A. Peart, "Aircraft Noise Source and Contour Estimation," NASA, Boeing Commercial Airplane Co. Seattle, WA, United States, Contractor Report (CR) NASA-CR-114649, 1973.

[81] G. J. Bennett, J. Lai, G. O'Brien, D. Ragni, F. Avallone, and M. Pott-Pollenske, "Flow Control and Passive Low Noise Technologies for Landing Gear Noise Reduction," in *28th AIAA/CEAS Aeroacoustics 2022 Conference*, ser. Aeroacoustics Conferences, American Institute of Aeronautics and Astronautics, Jun. 2022. DOI: 10.2514/6.2022-2848.

[82] J. W. Russel, "An empirical method for predicting the mixing noise levels of subsonic circular and coaxial jets," NASA, Langley Research Center, Hampton, VA, United States, Contractor Report (CR) NASA-CR-3786, 1984.

[83] C. Tam and N. Pastouchenko, "Gap tones - A component of airframe noise," in *38th Aerospace Sciences Meeting and Exhibit*, Reno, Nevada: American Institute of Aeronautics and Astronautics, Jan. 2000. DOI: 10.2514/6.2000-606.

[84] M. R. Fink, "Airframe Noise Prediction Method," en, Federal Aviation Administration (FAA), Washington, D.C., Tech. Rep. FAA-RD-77-29, 1977.

[85] N. Molin, "Airframe noise modeling and prediction," en, *CEAS Aeronautical Journal*, vol. 10, no. 1, pp. 11–29, Mar. 2019, ISSN: 1869-5590. DOI: 10.1007/s13272-019-00375-4.

[86] M. R. Fink, "Noise Component Method for Airframe Noise," *Journal of Aircraft*, vol. 16, no. 10, pp. 659–665, Oct. 1979, Publisher: American Institute of Aeronautics and Astronautics, ISSN: 0021-8669. DOI: 10.2514/3.58586.

[87] I. C. Dedoussi, T. P. Hynes, and H. A. Siller, "Investigating landing gear noise using fly-over data: The case of a Boeing 747-400," in *19th AIAA/CEAS Aeroacoustics Conference*, Berlin, Germany: American Institute of Aeronautics and Astronautics, May 2013. DOI: 10.2514/6.2013-2115.

[88] A. Hajczak, L. Sanders, and P. Druault, "Landing gear interwheel tonal noise characterization with the Boundary Element Method," *Journal of Sound and Vibration*, vol. 458, pp. 44–61, Oct. 2019, ISSN: 0022-460X. DOI: 10.1016/j.jsv.2019.06.010.

[89] R. Sen, B. Hardy, K. Yamamoto, Y.-P. Guo, and G. Miller, "Airframe Noise Sub-Component Definition and Model," NASA, Langley Research Center, Hampton, Virginia, Contractor Report (CR) NASA/CR-2004-213255, 2004.

[90] Y. Guo, "Empirical Prediction of Aircraft Landing Gear Noise," NASA Langley Research Center Hampton, VA, United States, Contractor Report NASA-CR-2005-213780, Jul. 2005.

[91] Y. Guo, C. L. Burley, and R. H. Thomas, "Landing Gear Noise Prediction and Analysis for Tube-And-Wing and Hybrid-Wing-Body Aircraft," in *54th AIAA Aerospace Sciences Meeting*, San Diego, California, USA: American Institute of Aeronautics and Astronautics, Jan. 2016, ISBN: 978-1-62410-393-3. DOI: 10.2514/6.2016-1273.

[92] Y. P. Guo, K. J. Yamamoto, and R. W. Stoker, "Experimental Study on Aircraft Landing Gear Noise," *Journal of Aircraft*, vol. 43, no. 2, pp. 306–317, 2006, ISSN: 0021-8669. DOI: 10.2514/1.11085.

[93] R. E. Owens, "Energy efficient engine: Propulsion system-aircraft integration evaluation," Contractor Report (CR) NASA-CR-159488, Mar. 1979.

[94] D. Casalino, F. Diozzi, R. Sannino, and A. Paonessa, "Aircraft noise reduction technologies: A bibliographic review," *Aerospace Science and Technology*, vol. 12, no. 1, pp. 1–17, Jan. 2008. DOI: 10.1016/j.ast.2007.10.004.

[95] E. Envia, "Fan Noise Reduction: An Overview," in *39th Aerospace Sciences Meeting and Exhibit*, Reno, Nevada: American Institute of Aeronautics and Astronautics, 2001. DOI: 10.2514/6.2001-661.

[96] L. Leylekian, M. Lebrun, and P. Lempereur, "An overview of aircraft noise reduction technologies," *Aerospace Lab, Alain Appriou*, no. 7, pp. 1–15, Jun. 2014. DOI: 10.12762/2014.AL07-01.

[97] E. A. Krejsa and J. R. Stone, "Enhanced Fan Noise Modeling for Turbofan Engines," Diversitech, Inc., Cincinnati, OH, United States, Contractor Report NASA/CR—2014-218421, Dec. 2014.

[98] E. A. Krejsa, "New technique for the direct measurement of core noise from aircraft engines," NASA-TM-82634, Colorado Springs, Colorado: NASA, Jul. 1981.

[99] J. Mendoza, D. Nance, and K. Ahuja, "Source Separation from Multiple Microphone Measurements in the Far Field of a Full Scale Aero Engine," in *14th AIAA/CEAS Aeroacoustics Conference (29th AIAA Aeroacoustics Conference)*, ser. Aeroacoustics Conferences, Vancouver, British Columbia: American Institute of Aeronautics and Astronautics, May 2008. DOI: 10.2514/6.2008-2809.

[100] L. Hultgren, "A Comparison of Combustor-Noise Models," in *18th AIAA/CEAS Aeroacoustics Conference (33rd AIAA Aeroacoustics Conference)*, NASA/TM - 2012 - 217671, Colorado Springs, Colorado, Jun. 2012, ISBN: 978-1-60086-932-7. DOI: 10.2514/6.2012-2087.

[101] J. R. Stone, E. A. Krejsa, and B. J. Clark, "Enhanced Core Noise Modeling for Turbofan Engines," Contractor Report (CR) NASA-CR-2011-217026, Jun. 2011.

[102] J. J. Emmerling, "Core Engine Noise Control Program, Volume III, Supplement 1—Prediction Methods," Federal Aviation Administration (FAA), Springfield, Virginia, Tech. Rep. FAA RD-74-125 III-I, Mar. 1976.

[103] P. Ho and V. Doyle, "Combustion noise prediction update," in *5th Aeroacoustics Conference*, ser. Aeroacoustics Conferences, American Institute of Aeronautics and Astronautics, Mar. 1979. DOI: 10.2514/6.1979-588.

[104] J. R. Stone, "Interim prediction method for jet noise," Tech. Rep. E-8112, Jan. 1974, NASA-TM-X-71618. [Online]. Available: https://ntrs.nasa.gov/citations/19740027003 (visited on 01/30/2024).

[105] S. P. Pao, *A correlation of mixing noise from coannular jets with inverted flow profiles*, NASA-TP-1301, Apr. 1979.

[106] M. R. Khorrami and D. P. Lockard, "Effects of Geometric Details on Slat Noise Generation and Propagation," LF99-8604, Jan. 2009.

[107] J. Mendoza, T. Brooks, and W. Humphreys, "Aeroacoustic Measurements of a Wing/Slat Model," in *8th AIAA/CEAS Aeroacoustics Conference & Exhibit*, Breckenridge, Colorado: American Institute of Aeronautics and Astronautics, Jun. 2002. DOI: 10.2514/6.2002-2604.

[108] Y. Guo, "Aircraft Flap Side Edge Noise Modeling and Prediction," in *17th AIAA/CEAS Aeroacoustics Conference (32nd AIAA Aeroacoustics Conference)*, ser. Aeroacoustics Conferences, Portland, Oregon: American Institute of Aeronautics and Astronautics, Jun. 2011. DOI: 10.2514/6.2011-2731.

[109] T. F. Brooks and W. M. Humphreys, "Flap-edge aeroacoustic measurements and predictions," *Journal of Sound and Vibration*, vol. 261, no. 1, pp. 31–74, Mar. 2003, ISSN: 0022-460X. DOI: 10.1016/S0022-460X(02)00939-2.

[110] N. Molin, M. Roger, and S. Barre, "Prediction of Aircraft High-Lift Device Noise Using Dedicated Analytical Models," in *9th AIAA/CEAS Aeroacoustics Conference and Exhibit*, ser. Aeroacoustics Conferences, Hilton Head, South Carolina: American Institute of Aeronautics and Astronautics, May 2003. DOI: 10.2514/6.2003-3225.

[111] Y. Guo, "Slat noise modeling and prediction," *Journal of Sound and Vibration*, vol. 331, no. 15, pp. 3567–3586, Jul. 2012, ISSN: 0022-460X. DOI: 10.1016/j.jsv.2012.03.016.

[112] W. Dobrzynski and M. Pott-Pollenske, "Slat noise source studies for farfield noise prediction," in *7th AIAA/CEAS Aeroacoustics Conference and Exhibit*, Maastricht, Netherlands: American Institute of Aeronautics and Astronautics, May 2001. DOI: 10.2514/6.2001-2158.

[113] M. R. Khorrami, W. M. Humphreys, D. P. Lockard, and P. A. Ravetta, "Aeroacoustic Evaluation of Flap and Landing Gear Noise Reduction Concepts," NF1676L-17628, Atlanta, GA: NASA, Jun. 2014.

[114] Y. Guo, "On noise reduction by flap side edge fences," *Journal of Sound and Vibration*, vol. 277, no. 1, pp. 369–390, Oct. 2004, ISSN: 0022-460X. DOI: 10.1016/j.jsv.2003.09.029.

[115] Y. Zhang, A. O'Neill, L. N. Cattafesta, K. Pascioni, M. M. Choudhari, M. R. Khorrami, D. P. Lockard, and T. Turner, "Assessment of Noise Reduction Concepts for Leading-Edge Slat Noise," NF1676L-30046, Atlanta, GA, Jun. 2018.

[116] K. Zhao, P. Okolo, E. Neri, P. Chen, J. Kennedy, and G. J. Bennett, "Noise reduction technologies for aircraft landing gear-A bibliographic review," *Progress in Aerospace Sciences*, vol. 112, p. 100 589, Jan. 2020, ISSN: 0376-0421. DOI: 10.1016/j.paerosci.2019.100589.

[117] R. M. Yupa-Villanueva, F. D. da Silva, and C. J. Deschamps, "Effects of Jet–Flap Interaction on Flow and Acoustic Fields," *Flow, Turbulence and Combustion*, Jun. 2023, ISSN: 1573-1987. DOI: 10.1007/s10494-023-00435-0.

[118] J. Lawrence, "Aeroacoustic interactions of installed subsonic round jets," Ph.D. Thesis, University of Southampton, Jul. 2014. [Online]. Available: https://eprints.soton.ac.uk/367059/ (visited on 01/31/2024).

[119] C. A. Brown, "Jet-Surface Interaction Test: Far-Field Noise Results," *Journal of Engineering Gas Turbines and Power*, vol. 135, no. 7, Jun. 2013, GTP-12-1222. DOI: 10.1115/1.4023605.

[120] S. Salehian and R. Mankbadi, "Jet Noise in Airframe Integration and Shielding," *Applied Sciences*, vol. 10, no. 2, p. 511, Jan. 2020, Number: 2 Publisher: Multidisciplinary Digital Publishing Institute, ISSN: 2076-3417. DOI: 10.3390/app10020511.

[121] J. Sementi, "Jet exhaust and wing flap interactions," in *40th AIAA Aerospace Sciences Meeting & Exhibit*, Reno, Nevada: American Institute of Aeronautics and Astronautics, Jan. 2002. DOI: 10.2514/6.2002-17.

[122] F. V. Hutcheson, D. Stead, and G. Plassman, "Experimental Study of Wake / Flap Interaction Noise and the Reduction of Flap Side Edge Noise," in *22nd AIAA/CEAS Aeroacoustics Conference*, ser. Aeroacoustics Conferences, NF1676L-22656, Lyon, France: American Institute of Aeronautics and Astronautics, May 2016. DOI: 10.2514/6.2016-2955.

[123] S. Oerlemans and M. Pott-Pollenske, "An experimental study of landing gear wake/flap interaction noise," en, National Aerospace Laboratory NLR, Amsterdam, The Netherlands, Tech. Rep. NLR-TP-2004-318, Aug. 2004, Publisher: National Aerospace Laboratory NLR.

[124] A. Vieira, M. Snellen, and D. G. Simons, "Assessing the shielding of engine noise by the wings for current aircraft using model predictions and measurements," en, *The Journal of the Acoustical Society of America*, vol. 143, no. 1, pp. 388–398, Jan. 2018, ISSN: 0001-4966, 1520-8524. DOI: 10.1121/1.5020798.

[125] J. J. Berton, "Noise Reduction Potential of Large, Over-the-Wing Mounted, Advanced Turbofan Engines," NASA Glenn Research Center, Cleveland, OH, United States, Manuscrtipt TM-2000-210025, Apr. 2000.

[126] Y. Guo, C. L. Burley, and R. H. Thomas, "On Noise Assessment for Blended Wing Body Aircraft," NF1676L-16686, National Harbor, MD: American Institute of Aeronautics and Astronautics, Jan. 2014. DOI: 10.2514/6.2014-0365.

[127] R. Pieren, I. Le Griffon, L. Bertsch, A. Heusser, F. Centracchio, D. Weintraub, C. Lavandier, and B. Schäffer, "Perception-based noise assessment of a future blended wing body aircraft concept using synthesized flyovers in an acoustic VR environment—The ARTEM study," *Aerospace Science and Technology*, vol. 144, p. 108 767, Jan. 2024, ISSN: 1270-9638. DOI: 10.1016/j.ast.2023.108767.

[128] M. R. Wilson, "An introduction to high speed aircraft noise prediction," Lockheed Engineering and Sciences Co., Hampton, VA, United States, Contractor Report NASA-CR-189582, Feb. 1992.

[129] C. Zellmann, B. Schäffer, J. M. Wunderli, U. Isermann, and C. O. Paschereit, "Aircraft Noise Emission Model Accounting for Aircraft Flight Parameters," *Journal of Aircraft*, vol. 55, no. 2, pp. 682–695, 2018, ISSN: 0021-8669. DOI: 10.2514/1.C034275.

[130] W. Krebs, R. Bütikofer, S. Plüss, and G. Thomann, "Spectral Three-Dimensional Sound Directivity Models for Fixed Wing Aircraft," *Acta Acustica united with Acustica*, vol. 92, no. 2, pp. 269–277, Mar. 2006.

[131] G. G. Fleming, D. A. Senzig, D. A. McCurdy, C. J. Roof, and A. S. Rapoza, "Engine Installation Effects of Four Civil Transport Airplanes: Wallops Flight Facility Study," Technical Memorandum (TM) TM-2003-212433, Oct. 2003.

[132] J. Wunderli, J. Meister, D. Jäger, S. Schalcher, C. Zellmann, and B. Schäffer, "Aircraft noise in situations with grazing sound incidence—Comparing different modeling approaches," *The Journal of the Acoustical Society of America*, vol. 151, pp. 3140–3151, May 2022. DOI: 10.1121/10.0010419.

[133] SAE Aerospace, "Method for Predicting Lateral Attenuation of Airplane Noise," SAE International, Aerospace Information Report SAE AIR 5662 Rev. D, Apr. 2006.

[134] D. G. Crighton, J. E. F. Williams, and l. C. Cheeseman, "The Outlook for Simulation of Forward Flight Effects on Aircraft Noise," *Journal of Aircraft*, vol. 14, no. 11, pp. 1117–1125, Nov. 1977, Publisher: American Institute of Aeronautics and Astronautics, ISSN: 0021-8669. DOI: 10.2514/3.58899.

[135] R. S. Larson, "Convective amplification of gas turbine engine internal noise sources," *Journal of Sound and Vibration*, vol. 74, no. 1, pp. 123–137, Jan. 1981, ISSN: 0022-460X. DOI: 10.1016/0022-460X(81)90496-X.

[136] ISO, "Acoustics - Attenuation of sound during propagation outdoors Part 1: Calculation of the absorption of sound by the atmosphere," Standard, International Organization of Standarizations, Tech. Rep. ISO 9613-1:1993, 1993.

[137] C. F. Chien and W. W. Soroka, "Sound propagation along an impedance plane," *Journal of Sound and Vibration*, vol. 43, no. 1, pp. 9–20, Nov. 1975. DOI: 10.1016/0022-460X(75)90200-X.

[138] M. E. Delany and E. N. Bazley, "Acoustical properties of fibrous absorbent materials," *Applied Acoustics*, vol. 3, no. 2, pp. 105–116, Apr. 1970. DOI: 10.1016/0003-682X(70)90031-9.

[139] J. E. Piercy and T. F. W. Embleton, "Review of sound propagation in the atmosphere," en, *Canadian Acoustics*, vol. 10, no. 1, pp. 24–37, Jan. 1982, Number: 1, ISSN: 2291-1391.

[140] J. Boettcher, *Annex 16, Volume I and equivalent procedure*, Bangkok, 2006. [Online]. Available: https://www.icao.int/Meetings/EnvironmentalWorkshops/Documents/NoiseCertificationWorkshop-2004/BIP_2_2_jb.pdf (visited on 04/24/2024).

[141] M. Vorländer, *Auralization - Fundamentals of Acoustics, Modelling, Simulation, Algorithms and Acoustic Virtual Reality* (RWTHedition), 2nd ed. Cham, Switzerland: Springer, 2020, ISBN: 978-3-030-51202-6.

[142] S. A. Rizzi and A. K. Sahai, "Auralization of air vehicle noise for community noise assessment," *CEAS Aeronautical Journal*, vol. 10, pp. 313–334, 2019. DOI: 10.1007/s13272-019-00373-6.

[143] E. C. Ifeachor and B. W. Jervis, *Digital Signal Processing - A Practical Approach*. Boston: Assison-Wesley Publishing Company, 1993, ISBN: 0-201-54413-X.

[144] U. ölzer, *DAFX: Digital Audio Effects - Second Edition*. West Sussex,UK: John Wiley & Sons Ltd, 2011, ISBN: 978-0-470-66599-2.

[145] S. W. Smith, *The Scientist &Engineer's Guide to Digital Signal Processing - Second Edition*. CA, United States: California Technical Publishing, 1999, ISBN: 0-9660176-7-6.

[146] M. Arntzen, "Aircraft noise calculation and synthesis in a non-standard atmosphere," ISBN-978-94-6259-464-7, Ph.D. Thesis, Delft University of Technology, Delft, the Netherlands, 2014.

[147] S. Rizzi and B. Sullivan, "Synthesis of Virtual Environments for Aircraft Community Noise Impact Studies," en, in *11th AIAA/CEAS Aeroacoustics Conference*, Monterey, California: American Institute of Aeronautics and Astronautics, May 2005, ISBN: 978-1-62410-052-9. DOI: 10.2514/6.2005-2983.

[148] F. Rietdijk, "Auralisation of airplanes considering sound propagation in a turbulent atmosphere," Ph.D. Thesis, Chalmers University of Technology, Gothenburg, Sweden, 2017.

[149] K. Heutschi, R. Pieren, M. Müller, M. Manyoky, U. Wissen Hayek, and K. Eggenschwiler, "Auralization of wind turbine noise: Propagation filtering and vegetation noise synthesis," *Acta Acustica united with Acustica*, vol. 100, no. 1, pp. 13–24, Jan. 2014, ISSN: 16101928. DOI: 10.3813/AAA.918682.

[150] S. A. Rizzi and A. Christian, "A method for simulation of rotorcraft fly-in noise for human response studies," NF1676L-21045, San Francisco, CA, Aug. 2015.

[151] M. Åbom, A. Johansson, K. Bolin, and S. Basu, "Approach Noise Trials," KTH Royal Institute of Technology, Stockholm, Sweden, Technical report for the KTH/Novair project Approach Noise Trials (ANT), Apr. 2021. [Online]. Available: https://www.kth.se/polopoly_fs/1.1139614.%201643808790!/Approach%20Noise%20Trials_Report.pdf (visited on 12/05/2023).

[152] L. Godby, "ANOPP validation study: Lockheed L-1011," Lockheed-California Co., Burbank, CA, United States, Contractor Report NASA-CR-159138, Oct. 1979.

[153] J. S. Gray, J. T. Hwang, J. R. R. A. Martins, K. T. Moore, and B. A. Naylor, "OpenMDAO: An open-source framework for multidisciplinary design, analysis, and optimization," *Structural and Multidisciplinary Optimization*, vol. 59, pp. 1075–1104, 2019.

[154] J. E. Green, "Greener by Design — the technology challenge," *The Aeronautical Journal*, vol. 106, no. 1056, pp. 57–113, Feb. 2002. DOI: 10.1017/S0001924000095993.

[155] *SAFT*, Feb. 2022. [Online]. Available: https://www.kth.se/csa/projekt/avslutade-projekt/saft-1.991973 (visited on 04/27/2022).

[156] G. F. Greco, R. Merino-Martínez, and A. Osses, *SQAT: A sound quality analysis toolbox for MATLAB*, May 2023. [Online]. Available: https://zenodo.org/records/7934710#.ZGD-H3ZBxhF (visited on 03/02/2024).

[157] *Chalmers Research*. [Online]. Available: https://research.chalmers.se/en/ (visited on 03/06/2024).

Appendix A
Audio files

In Section 5.6, auralizations and recordings of flyover aircraft in approach conditions were presented and discussed. The comparison was performed in terms of spectrograms, sound exposure level, maximum noise level and sound pressure level time history. The corresponding sound files can be downloaded by searching for the electronic version of the thesis in the Chalmers Research website [157].

The sound files are named based on the respective figure where their spectrograms are presented. The duration of each sound file is 20 seconds, with a starting time approximately 10 seconds before the synthesized maximum A-weighted sound pressure level is reached. The starting time for each audio file is also indicated in the name. Furthermore, the word "synthesized" or "measured" can be found in the name of each file, indicating whether it corresponds to a synthesized case or a recording. A list of the available sound files is presented in Table A.1. It should be noted that during the recordings the microphones were not calibrated at the typical 94 $dB\ SPL$ level, but 100.2 dB was used. Therefore, both the recorded and synthesized audio files assume 100.2 $dB\ SPL$ for the full-scale amplitude. The results presented in Section 5.6 have been re-calibrated to 94 dB. It is, generally, recommended to listen to the files in an environment with relatively low background noise and to use headphones.

When listening to the auralized and recorded audio files, the observations that were made in Section 5.6 become evident. The amplitude modulations caused by the atmospheric turbulence are clearly audible in the recording, as are the differences in tonal components. Another distinct difference that is noticed when listening to the files is the binaural effect in the recording which is not included in the auralization.

Table A.1: Audio files.

Filename	Description
fig5.3_synthesized_7.50.23.wav	Synthesized flyover presented in Figure 5.3a
fig5.3_measured_7.50.23.wav	Recorded flyover presented in Figure 5.3b
fig5.4_synthesized_8.48.00.wav	Synthesized flyover presented in Figure 5.4a
fig5.4_measured_8.48.00.wav	Recorded flyover presented in Figure 5.4b
fig5.5_synthesized_8.3.47.wav	Synthesized flyover presented in Figure 5.5a
fig5.5_measured_8.3.47.wav	Recorded flyover presented in Figure 5.5b